Novel Polyoxoanion- and Bu_4N^+-Stabilized, Isolable, and Redissolvable, 20–30-Å $Ir_{\sim 300-900}$ Nanoclusters: The Kinetically Controlled Synthesis, Characterization, and Mechanism of Formation of Organic Solvent-Soluble, Reproducible Size, and Reproducible Catalytic Activity Metal Nanoclusters

Yin Lin[†] and Richard G. Finke*

Contribution from the Department of Chemistry, Colorado State University, Fort Collins, Colorado 80523

Received January 26, 1994[⊗]

Abstract: Nearly monodispersed 30 ± 4 Å $Ir_{\sim 900}$ nanoclusters have been prepared by hydrogen reduction of a polyoxoanion-supported Ir(I) complex, $(Bu_4N)_5Na_3[(1,5\text{-COD})Ir\cdot P_2W_{15}Nb_3O_{62}]$ (1,5-COD is 1,5-cyclooctadiene), in acetone solution. The $Ir_{\sim 900}$ nanoclusters can be isolated as a black powder and redissolved in acetone or CH_3CN to give a stable, amber solution. Extensive characterizations of the $Ir_{\sim 900}$ nanoclusters have been made by means of TEM, electron diffraction, electrophoresis, ultracentrifugation solution molecular-weight measurements, fast-atom bombardment mass spectroscopy, elemental analysis, and IR and UV–vis spectroscopy; their *average* chemical composition is $[Ir(0)_{\sim 900}(P_4W_{30}Nb_6O_{123}{}^{16-})_{\sim 60}](Bu_4N)_{\sim 660}Na_{\sim 300}$, in which the polyoxoanion is found to be in its oxidized and Nb–O–Nb bridged aggregate form, $P_4W_{30}Nb_6O_{123}{}^{16-}$. Electron diffraction studies show that the nanoclusters consist of cubic close-packed (ccp) Ir metal cores; electrophoresis and other techniques establish that the nanoclusters are stabilized in solution by the adsorption of the polyoxoanions on their outer surfaces. Smaller, ca. 20-Å $Ir_{\sim 300}$ nanoclusters have also been reproducibly prepared and characterized from $(Bu_4N)_5Na_3[(1,5\text{-COD})Ir\cdot P_2W_{15}Nb_3O_{62}]$ and from $(Bu_4N)_4Na_2[(1,5\text{-COD})Ir\cdot SiW_9Nb_3O_{40}]$ during the catalytic hydrogenation of cyclohexene; the average chemical composition of the $Ir_{\sim 300}$ nanoclusters isolated from $(Bu_4N)_5Na_3[(1,5\text{-COD})Ir\cdot P_2W_{15}Nb_3O_{62}]$ is $[Ir(0)_{\sim 300}(P_4W_{30}Nb_6O_{123}{}^{16-})_{\sim 33}](Bu_4N)_{\sim 300}Na_{\sim 233}$. The $Ir_{\sim 300}$ nanoclusters are unusual in their unexpected ±10% kinetic reproducibility in catalysis (cyclohexene hydrogenation) and also in their stability including their isolability. In addition, the $Ir_{\sim 300}$ nanoclusters catalyze the reduction of polyoxoanions to give intense blue, W^V-containing, "heteropolyblue" species. Evidence supporting a homogeneous nucleation, then autocatalytic growth mechanism for the formation of the nearly monodispersed Ir nanoclusters is also presented and discussed. The autocatalysis is the key to the separation in time of the nanocluster nucleation and growth steps; this separation is, in turn, an essential component for the formation of monodispersed nanoclusters (i.e., in the absence of micellar or other nanocluster growth-inhibiting microstructures).

Introduction

Well-characterized, stable transition metal nanoclusters[1] of a narrow size distribution (ideally single sized or monodispersed[2]) are of significant interest both fundamentally[3] and practically, for example, in catalysis.[4] Unfortunately, general routes to the synthesis of monodispersed metal particles are not yet available, largely because the *mechanisms* of formation of such nanoclusters or colloids[2,3c,5] are still poorly understood. The lack of general syntheses to homogeneous, monodispersed transition metal nanoclusters means, in turn, that the compositions—and therefore

[†] Based on the Ph.D. thesis of Y. Lin, March 1994 Department of Chemistry, University of Oregon, Eugene, OR 97403.

[⊗] Abstract published in *Advance ACS Abstracts*, July 1, 1994.

(1) (a) *Physics and Chemistry of Small Clusters*; Jena, P., Rao, B. K., Khanna, S. N., Eds.; Plenum Press: New York, 1987. (b) Andres, R. P.; Averback, R. S.; Brown, W. L.; Brus, L. E.; Goddard, W. A.; Kaldor, A.; Louie, S. G.; Moscovits, M.; Peercy, P. S.; Riley, S. J.; Siegel, R. W.; Spaepen, F.; Wang, Y. *J. Mater. Res.* **1989**, *4*, 704. This is a Panel Report from the Department of Energy, Council on Materials Science on "Research Opportunities on Clusters and Cluster-assembled Materials". (c) Thomas, J. M. *Pure Appl. Chem.* **1988**, *60*, 1517–28. (d) Henglein, A. *Chem. Rev.* **1989**, *89*, 1861–1873. (e) A superb series of papers, complete with a record of the insightful comments by the experts attending the conference, is available in: *Faraday Discuss. Chem. Soc.* **1991**, *92*, 1–300.

(2) (a) Beattie, J. K. *Pure Appl. Chem.* **1989**, *61*, 937–41. (b) Matijevic, E. *Chem. Mater.* **1993**, *5*, 412. This paper contains an especially valuable discussion of the (poor) state of understanding of the mechanisms of formation of monodispersed particles.

(3) (a) Lin, M. Y.; Lindsay, H. M.; Weitz, D. A.; Ball, R. C.; Klein, R.; Meakin, P. *Nature* **1989**, *339*, 360. (b) Ottewill, R. H. *Faraday Discuss. Chem. Soc.* **1990**, *90*, 1. (c) Look, J.-L.; Bogush, G. H.; Zukoski, C. F. *Faraday Discuss. Chem. Soc.* **1990**, *90*, 345.

(4) (a) Gates, B. C., Guczi, L., Knozinger, H., Eds.; *Metal Clusters in Catalysis*; Elsevier: New York, 1986. (b) Schmid, G. *Aspects Homogeneous Catal.* **1990**, *7*, 1–36.

(5) (a) LaMer, V. K.; Dinegar, R. H. *J. Am. Chem. Soc.* **1950**, *72*, 4847; see, also: LaMer, V. K. *Ind. Eng. Chem.* **1952**, *44*, 1270. This classic work on the nucleation steps in the formation of monodispersed particles has, however, been labeled as too simplistic to account for the facts that are now available (and has also been hinted at as "overcited").[2b] (b) Van Rheenen, P. R.; McKelvy, M. J.; Glaunsinger, W. S. *J. Solid State Chem.* **1987**, *67*, 151. This paper discusses the classical law (von Weimarn's law) which relates concentration to growth *of a precipitate*. It is not directly relevant to the present work since, although we do see a precipitate, it is formed long after our cluster size-determining steps are over). (c) Steigerwald. M. L.; Brus, L. *Acc. Chem. Res.* **1990**, *23*, 183. (d) Lin, M. Y.; Lindsay, H. M.; Weitz, D. A.; Ball, R. C.; Klein, R.; Meakin, P. *Nature* **1989**, *339*, 360. (e) Melrose, J. R. *J. Chem. Phys.* **1990**, *92*, 4595. (f) Fojtik, A.; Weller, H.; Koch, U.; Henglein, A. *Ber. Bunsen-Ges. Phys. Chem.* **1984**, *88*, 969. (g) Several quotes from an excellent 1993 review[2b] of uniform size colloids (Matijevic, E. *Chem. Mater.* **1993**, *5*, 412), ones generally made by a precipitation processes, make apparent the need for additional, quantitative mechanistic studies within the general area of monodispersed colloids. "The ultimate aim in the studies of chemical mechanisms in the precipitations from homogeneous solutions is to develop some general principles, that would make predictable the processes leading to the formation of uniform particles". Another noteworthy paragraph is the following: "The quantitative explanation of a process by which a huge number of subunits aggregate into *identical* large particles has not been developed as of yet. It is also not clear why in some instances the final particles are spherical and in others they appear in different geometric forms, yet are of the same chemical composition". And a final interesting quote is "One of the most vexing problems of fine particle science, which has ramifications in many other areas (e.g., geology, crystallography, etc.) is related to particle morphology. ... In many cases there is no rational to explain the appearance of a given particle morphology".

0002-7863/94/1516-8335$04.50/0

the structures—of most nanoclusters are also poorly defined, especially since many past syntheses did not bother to exclude oxygen.[6] Often, even the *average* chemical composition or the overall charge of a "colloid" or "nanocluster" is not known with certainty and can only be guessed at as "$[M_aH_bO_c(OH)_dX_e$-(polymer coating)$_f]^{x+/-}$" (H = hydrides; X = halides). Note, here, how much simpler the compositional characterization of a metal colloid would be if oxygen, water, and halides (and thus O_2, OH^-, and X^- ligands) are avoided during their synthesis.

There is even confusion in the literature regarding the nomenclature used to describe small metal aggregates: the terms clusters, nanoclusters, or colloids have all been used to describe metal aggregates of sometimes quite different size or composition (see also Bradley's discussion of this nomenclature problem[7]). Although any definition is somewhat arbitrary due to the *continuum* of increasing metal aggregation states in principle possible, we will adopt Schmid's definition[8] (see the footnote for further details)[9] in which metal *nanoclusters* are unambiguously defined as those metal aggregates smaller than 100 Å (i.e., 10 nm) in diameter and metal colloids are defined as those aggregates bigger than 100 Å (and which also typically have a broader size distribution). Hence, the 20–30-Å (i.e., 2–3 nm) Ir particles described in the present paper will be referred to as iridium nanoclusters.

Historically, colloids and nanoclusters have been prepared in aqueous solutions in the presence of stabilizing agents, resulting in either so-called "charge stabilization" (e.g., by the adsorption of ions such as Cl^-) or "steric stabilization" (e.g., by the surface adsorption of polymers) (Figure 1).[10,11] Surface-adsorbed halides or polymers kinetically stabilize colloids by inhibiting further particle aggregation. A literature example relevant to the present work is the collection of Ir nanoclusters prepared by refluxing a methanol–water solution of Na_2IrCl_6 in the presence of poly(vinyl alcohol). However, the exact composition of the resulting nanoclusters is unknown, "$[Ir_aH_bO_c(OR)_dCl_e$(poly(vinyl alcohol))$_f]^{x+/-}$" (R = Me, H).[12a] The transmission electron micrograph and the frequency vs size histogram of the Ir nanoclusters (prepared in our hands using this literature procedure[12a]) are shown in Figure 2; the mean diameter of 17 Å (with standard deviation of 4 Å) is very similar to the literature report within experimental error (average diameter of 14 Å; no standard deviation was given).[12a] This traditional polymer-stabilized "Ir colloid", actually $Ir_{\sim 80-320}$ nanocluster,[12b,29] provides a valuable reference point for a later comparison to the Ir nanoclusters prepared herein.

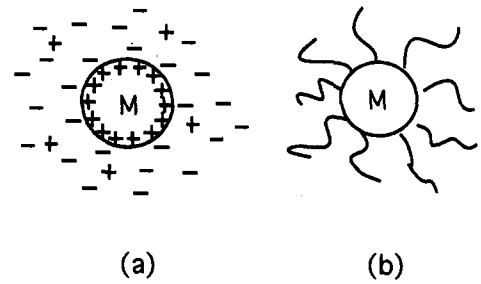

Figure 1. A schematic illustration for (a) an electrostatically stabilized metal (M) particle (i.e., one stabilized by the adsorption of ions and the resultant electrical double layer) and (b) a sterically stabilized metal particle (i.e., one stabilized by the adsorption of polymer chains).

In the last few years, there has been an explosive growth[13,14] in the number of reports of metal clusters or colloids prepared in *organic solvents*,[15] either by chemical reduction of simple metal salts[13] or by metal-vapor deposition.[14] In some cases the resultant metal aggregates are quite stable even in the absence of added polymer stabilizers.[13a,b,14d,e] An important example relevant to the present work is Bönnemann and co-workers' preparation[16] of ca. 1.5-nm[16c] Ir nanoclusters by a $N(Octyl)_4^+BEt_3H^-$ reduction of $IrCl_3$ in THF and initially under an inert, O_2-free atmosphere (unfortunately, however, the nanoclusters were then worked up in air; the possible air-sensitivity of zero-valent metal nanoclusters is, surprisingly, apparently not a generally appreciated point). The resultant red–black Ir nanoclusters are very soluble in organic solvents such as THF or acetone; the solubility and the stability is attributed[16] to the presence of $N(Octyl)_4^+$ surrounding the Ir nanoclusters. However, the degree of polydispersity or range of the nanocluster sizes was not given, and again, neither the average

(6) (a) There is evidence that small metal aggregates can be air-sensitive. For example, Ir nanoclusters (10–20 Å) generated by radiolysis of $(NH_4)_2$-$IrCl_6$ form large aggregates of poorly characterized "$IrO_2{\cdot}xH_2O$" colloids after standing for several days in air, indicating that Ir nanoclusters are reactive toward oxygen and water.[6b] (b) Harriman, A.; Thomas, J. M. *Nouv. J. Chim.* **1987**, *11*, 757.

(7) Bradley, J. S.; Hill, E. W.; Behal, S.; Klein, C.; Chaudret, B.; Duteil, A. *Chem. Mater.* **1992**, *4*, 1234.

(8) Schmid, G. *Endeavour* **1990**, *14*, 172–8.

(9) The confusion surrounding the nomenclature of "colloids" and "clusters" is no doubt in part due to the continuum of increasing metal aggregation possible, ranging from discrete single-metal complexes, to clusters such as nanoclusters, then to higher clusters ("colloids"), and finally to the bulk metal, as shown below. (The lack of precise compositional, size, or purity data for many "clusters" or "colloids" undoubtedly also contributes to this nomenclature problem.) Schmid's dividing line at 100 Å between *nanoclusters* and larger, traditional colloids effectively avoids this confusion and is, therefore, adopted for the purposes of this work.[8]

Discrete, single-metal complexes	Metal clusters, including nanoclusters < 100 Å	Traditional metal colloids > 100 Å	Bulk metal

The continuum of metal aggregate sizes

(10) For a general discussion on the stability of colloids or nanoclusters, see, for example: (a) Hirtzel, C. S.; Rajagopalan, R. *Colloidal Phenomena: Advanced Topics*; Noyes Publications: New Jersey, 1985; pp 27–39, 73–87. (b) Hunter, R. J. *Foundations of Colloid Science*; Oxford University Press: New York, 1987; Vol. 1, pp 316–492.

(11) Examples of charged or polymer-stabilized colloids or nanoclusters in *aqueous solution* are as follows: (a) Faraday, M. *Philos. Trans. R. Soc. London* **1857**, *147*, 145. (b) Van Rheenen, P. R.; McKelvy, M. J.; Glaunsinger, W. S. *J. Solid State Chem.* **1987**, *67*, 151. (c) Nakao, Y.; Kaeriyama, K. *J. Colloid Interface Sci.* **1986**, *110*, 82. (d) Boutonnet, M.; Kizling, J.; Stenius, P.; Maire, G. *Colloids Surf.* **1982**, *5*, 209–25. (e) Schmid, G.; Lehnert, A. *Angew. Chem., Int. Ed. Engl.* **1989**, *28*, 780. (f) Natanson, G.; Amar, F.; Berry, R. S. *J. Chem. Phys.* **1983**, *78*, 399. (g) Nagata, Y.; Watananabe, Y.; Fujita, S.-I.; Dohmaru, T.; Taniguchi, S. *J. Chem. Soc., Chem. Commun.* **1992**, 1620. (h) Yeung, S. A.; Hobson, R.; Biggs, S.; Grieser, F. *J. Chem. Soc., Chem. Commun.* **1993**, 378. (j) Reference 6b.

(12) (a) Hirai, H.; Nakao, Y.; Toshima, N. *J. Macromol. Sci., Chem.* **1979**, *A13*, 727. (b) Assuming that the Ir nanoclusters are perfect spheres and that the packing (and thus the density) of the Ir atoms is the same as in the bulk Ir(0) metal, the nanoclusters with average diameter of 16.8 (± 3.7) Å can be approximated as Ir_{175}. Similarly 20.5-Å (i.e., 16.8 + 3.7) and 13.1-Å (i.e., 16.8 – 3.7) nanoclusters can be approximated as Ir_{320} and Ir_{80}, respectively. (See elsewhere for the equations used in these calculations.[29])

(13) (a) Esumi, K.; Tano, T.; Meguro, K. *Langmuir* **1989**, *5*, 268. (b) Lewis, L. N.; Lewis, N. *Chem. Mater.* **1989**, *1*, 106–14. (c) Satoh, N.; Kimura, K. *Bull. Chem. Soc. Jpn.* **1989**, *62*, 1758–63. (d) Bradely, J. S.; Hill, E. W.; Klein, C.; Chaudret, B.; Duteil, A. *Chem. Mater.* **1993**, *5*, 254. (e) Duteil, A.; Queau, R.; Chaudret, B. *Chem. Mater.* **1993**, *5*, 341. (f) Schueller, O. J. A.; Pocard, N. L.; Huston, M. E.; Spontak, R. J.; Neenan, T. X.; Callstrom, M. R. *Chem. Mater.* **1993**, *5*, 11.

(14) (a) Andrews, M. P.; Ozin, G. A. *Chem. Mater.* **1989**, *1*, 174 and the references herein. (b) Klabunde, K. J.; Habdas, J.; Cárdenas-Triviño, G. *Chem. Mater.* **1989**, *1*, 481. (c) Zuckerman, E. B.; Klabunde, K. J.; Olivier, B. J.; Sorensen, C. M. *Chem. Mater.* **1989**, *1*, 12–14. (d) Lin, S.-T.; Franklin, M. T.; Klabunde, K. J. *Langmuir* **1986**, *2*, 259. (e) Cárdenas-Triviño, G.; Klabunde, K. J.; Dale, E. B. *Langmuir* **1987**, *3*, 986–92. (f) Bradley, J. S.; Hill, E.; Leonowicz, M. E.; Witzke, H. *J. Mol. Catal.* **1987**, *41*, 59–74.

(15) (a) Actually, even in his Ph.D. thesis as early as 1905, Svedberg showed that more than 30 metal colloids could be produced in organic solvents like (wet?) isobutanyl alcohol or diethyl ether. (b) Stenius, P. In *Physical Chemistry of Colloids and Macromolecules*. Ranby, B., Ed.; Blackwell Scientific Publications: Oxford, U.K., 1987; p 17.

(16) (a) Bönnemann, H.; Brijoux, W.; Brinkmann, R.; Dinjus, E.; Joussen, T.; Korall, B. *Angew. Chem., Int. Ed. Engl.* **1991**, *30*, 1312. (b) These authors did report[16a] an elemental analysis (C, H, N, and Rh) for the cluster prepared from $RhCl_3$; the results accounted for 93.4% of the total weight (including 73.4% Rh), indicating that the remaining 6.6% is probably Cl^- and/or O^{2-}. (c) The average size of their Ir nanoclusters is 1.5 nm (Professor H. Bönnemann, private communication).

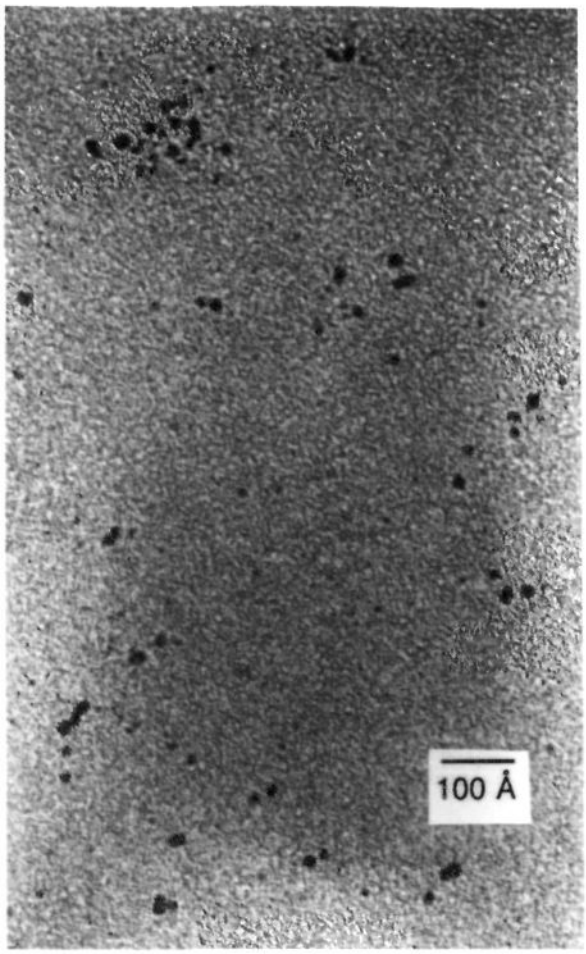

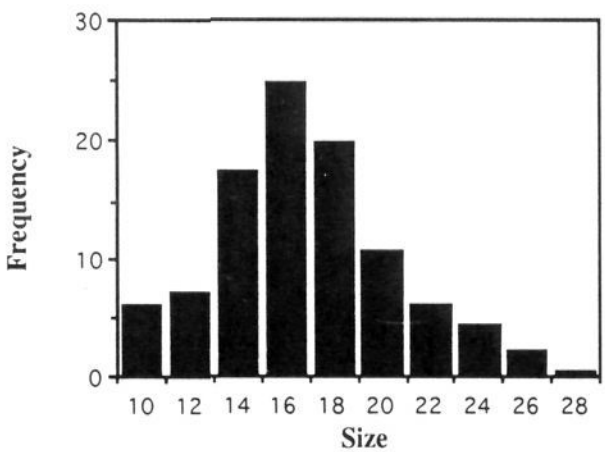

Figure 2. (A) (top) Transmission electron micrograph of Ir nanoclusters freshly prepared from refluxing Na_2IrCl_6 in alcohol/water in the presence of poly(vinyl alcohol) according to the literature.[12] (B) (bottom) Histogram of the Ir nanocluster diameters. The mean diameter is 16.8 Å with a standard deviation of 3.7 Å, from a sample population of 280.

composition[16b] nor the overall charge (positive or negative) of the Ir nanoclusters is known, "$[N(Octyl)_4^+]_x[\{Ir_aH_bO_c(OH)_dCl_e\}^{x-}]$".

Hence, and despite the recent advances in the synthesis and characterization of nanoclusters in organic solvents, important goals for research in this area include the following: (i) the development of highly kinetically controlled routes[5a,11b] for the preparation of metal particles of uniform sizes and shapes (and while rigorously excluding or controlling other key variables such as oxygen, water, halides, and protons); (ii) the development of synthetic routes to the so-called "magic number" clusters[17] (Figure 3) (as one excellent test of the efficacy of mechanism-based, kinetically controlled synthetic routes); (iii) the unequivocal characterization, including atomic-level structural characterization (ideally by X-ray crystallography[18]) of nanoclusters of different sizes; (iv) physicochemical studies leading to a better understanding of the often ill-defined surface compositions and structures of metal nanoclusters (for example, using a variety of spectroscopic methods[19-21]); (v) detailed studies of the role of key variables on the stability and chemical and physical properties of metal nanoclusters (specifically, variables such as O_2, H_2O, pH, R_4N^+ counterions, and different organic solvents or oligomeric or polymeric additives); (vi) additional mechanistic studies[2,5] of the kinetics of the nucleation, growth, and aggregation phases of nanocluster formation, with an eye toward developing routes to a given cluster of chosen dimensions; and (vii) studies of the applications of nanoclusters (again, ideally of uniform size), for example, their applications in catalysis.

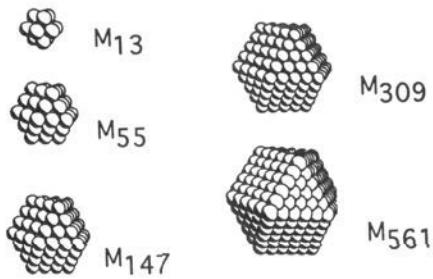

Figure 3. Idealized representation[17b] of hexagonal close-packed (hcp), full-shell clusters, termed "magic number" clusters in the literature. Note that the number of surface atoms for the nth shell is $10n^2 + 2$ for such twinned cubooctahedra structures with their hcp atoms. The same $10n^2 + 2$ formula is valid for cubooctahedra and their cubic close-packed atoms (ccp) (e.g., as in the relevant case of Ir(0) metal) and is also valid for icosahedral structures.[17a,f]

Herein we report our initial foray into the nanocluster area: the synthesis and characterization of novel polyoxoanion-dispersed

(17) (a) Teo, B. K.; Sloane, N. J. A. *Inorg. Chem.* **1985**, *24*, 4545. (b) Schmid, G.; Klein, N.; Morun, B.; Lehnert, A.; Malm, J. O. *Pure Appl. Chem.* **1990**, *62*, 1175–7. (c) Vargaftik, M. N.; Zagorodnikov, V. P.; Stolarov, I. P.; Moiseev, I. I.; Kochubey, D. I.; Likholobov, V. A.; Chuvilin, A. L.; Zamaraev, K. I. *J. Mol. Catal.* **1989**, *53*, 315. (d) The term "magic number" is controversial and probably somewhat misleading. A better term for these clusters may be "full-shell" clusters, that is, clusters which possess some extra stability in part simply due to their close-packed, full-shell nature where each Ir atom has the maximum number of nearest neighbors. (e) A good discussion of "magic number clusters", and especially of their validity in M_n cases (M = Na, K, Cs; n = 2, 8, 20, 40, 58, 92, 138, 196, 260, 344, 440, and 558), plus a good discussion the difference of these magic numbers from those based on icosahedral or cubooctahedral structures, are in the following: Howie, A. *Faraday Discuss.* **1991**, *92*, 1–11 (see p 2–3). (f) Wells, A. F. *Structural Inorganic Chemistry*, 4th ed.; Clarendon Press, Oxford, U.K., 1975. Pages 123 and 131 provide a concise discussion of sphere packings and their relationships to the 12 nearest neighbor atoms that define cubooctahedral (ccp or, equivalently, fcc) and twinned cubooctahedral (hcp) discrete structures.

(18) No X-ray crystallographic structural studies of clusters over M_{55} have appeared to date. However, there are reports[18b,c] that describe the use of high resolution TEM and STEM in an attempt to characterize Au_{55} and "Pd_{561}" giant metal clusters at near atomic level resolution. (But, problems exist in these studies including beam damage or reorganization of the metal cluster structure under the electron beam.) The use of STEM is still in its infancy for examining such giant clusters, as the resolution obtained to date is far from the atomic resolution that is in principle possible. (b) Schmid, G.; Klein, N.; Korste, L.; Kreibig, U.; Schönauer, D. *Polyhedron* **1988**, *7*, 605–8. (c) van de Leemput, L. E. C.; Gerritsen, J. W.; Rongen, P. H. H.; Smokers, R. T. M. *J. Vac. Sci. Technol.* **1991**, *B9*, 814.

(19) IR studies: (a) Bradley, J. S.; Hill, E. W.; Behal, S.; Klein, C. *Chem. Mater.* **1992**, *4*, 1234. (b) Bradley, J. S.; Millar, J. M.; Hill, E. W.; Behal, S. *J. Catal.* **1991**, *129*, 530–9. (c) Bradley, J. S.; Millar, J. M.; Hill, E. W. *J. Am. Chem. Soc.* **1991**, *113*, 4016–17. (d) Mucalo, M. R.; Cooney, R. P. *Chem. Mater.* **1991**, *3*, 1081.

(20) NMR studies: (a) Vargaftik, M. N.; Zagorodnikov, V. P.; Stolarov, I. P.; Moiseev, I. I.; Kochubey, D. I.; Likholobov, V. A.; Chuvilin, A. L.; Zamaraev, K. I. *J. Mol. Catal.* **1989**, *53*, 315–48. (b) Van, S. M. P. J.; Brom, H. B.; De, J. L. J.; Schmid, G. *Z. Phys. D: At., Mol. Clusters* **1989**, *12*, 451–2. (c) Reference 3b,c.

(21) EPR studies: Albino, J.; De, A. O.; Brom, H. B.; De, J. L. J.; Schmid, G. *Z. Phys. D: At., Mol. Clusters* **1989**, *12*, 457–9.

Ir nanoclusters, prepared from the hydrogen reduction in acetone of a compositionally well-defined, Cl^--free precursor, the polyoxoanion-supported organometallic complex,[22] $(Bu_4N)_5Na_3[(1,5\text{-}COD)Ir{\cdot}P_2W_{15}Nb_3O_{62}]$. The sharp distribution of reproducible size (ca. ±14%) Ir nanoclusters provides a catalytic activity reproducible (±10%) to a degree normally reserved for single-metal homogeneous catalysts.[23] Elsewhere we report the extensive mechanistic studies which led us to the discovery of the polyoxoanion/Bu_4N^+-stabilized nanoclusters reported herein.[24]

Results and Discussion

Preparation and Characterization of 30 ± 4 Å $Ir_{\sim 900}$ Nanoclusters (Sample I) Obtained by H_2 Reduction of $(Bu_4N)_5Na_3[(1,5\text{-}COD)Ir{\cdot}P_2W_{15}Nb_3O_{62}]$. The Ir nanoclusters herein were first discovered through our extensive mechanistic studies of the catalytic hydrogenation of cyclohexene in acetone beginning with $(Bu_4N)_5Na_3[(1,5\text{-}COD)Ir{\cdot}P_2W_{15}Nb_3O_{62}]$.[24,25] However, we subsequently discovered that the most convenient preparation, of what proved to be $Ir_{\sim 900}$ nanoclusters, is the direct reaction of $(Bu_4N)_5Na_3[(1,5\text{-}COD)Ir{\cdot}P_2W_{15}Nb_3O_{62}]$ (1 mM in acetone solution) with 40 psig (2.7 atm) of H_2.[26] As the reaction proceeds, Ir nanoclusters are gradually produced (ca. 30 Å, by TEM (Figures A and B, supplementary material), and the original clear-yellow solution gradually turns turbid-amber and then finally blue. The blue color is lost to give an amber solution within ca. 30 min if the H_2 atmosphere is released and when the solution is exposed to a N_2 atmosphere drybox (containing ≤1.0 ppm of O_2). (The blue color is due to the reduction of the polyoxoanion to form the well-known, reduced, W^V-containing heteropolyblue[27] as discussed in the next section.) A UV–visible spectrum (Figure C, supplementary material) of the amber solution shows no maximum but exhibits instead the trailing decrease in adsorption with increasing wavelength that is characteristic of light-scattering[28] (i.e., the plasmon resonance[28d]) of colloidal solutions.

The resultant 30.0 ± 4.1 Å Ir nanoclusters ($Ir_{\sim 640\text{-}1460}$) can be isolated by cyclohexane precipitation as a black powder (hereafter referred to as $Ir_{\sim 900}$ nanoclusters (sample I), *vide infra*).[29] Significantly, this black powder is still soluble in acetone and very soluble in CH_3CN. A transmission electron micrograph (Figure 4) of the isolated $Ir_{\sim 900}$ nanoclusters (sample I) in CH_3CN solution (sprayed onto a carbon-coated Cu grid) shows spherical Ir nanoclusters with an average diameter of 30.0 ± 4.1 Å (i.e., ±14%). This demonstrates that the nanoclusters are unchanged by the isolation procedure. The $Ir_{\sim 900}$ nanoclusters are about twice as big as, and somewhat more reproducible than, the 16.8 ± 3.7 Å (i.e., ±22%) Ir nanoclusters prepared by reducing Na_2IrCl_6 in the presence of poly(vinyl alcohol).[12] The transmission electron micrograph in Figure 4 also shows the presence of the polyoxoanion (the small granular particles) around the Ir nanoclusters. That these small particles are indeed polyoxoanions is demonstrated by the transmission electron micrographs of the $(Bu_4N)_9P_2W_{15}Nb_3O_{62}$ polyoxoanion and its Nb–O–Nb aggregate, $(Bu_4N)_{12}H_4P_4W_{30}Nb_6O_{123}$, as well as the polyoxoanion-supported $Ir(1,5\text{-}COD)^+$ complex $(Bu_4N)_5Na_3[(1,5\text{-}COD)Ir{\cdot}P_2W_{15}Nb_3O_{62}]$; all three compounds gave indistinguishable electron micrographs (Figure 5). The presence of the Nb–O–Nb bridged polyoxoanion $(Bu_4N)_{12}H_4P_4W_{30}Nb_6O_{123}$ in the isolated $Ir_{\sim 900}$·polyoxoanion nanoclusters (sample I) was further confirmed by IR and fast-atom bombardment mass spectroscopy, as discussed below. (Additional control experiments, described in the Experimental Section, demonstrate that the transmission electron micrographs shown throughout this paper are representative of the bulk sample and are not altered by changing the beam voltage or exposure times. Moreover, a control TEM of a carbon-film-coated Cu grid with no added sample confirms that the small granular particles are indeed the polyoxoanions.) Figure 6 is the large-area view of the Ir nanoclusters (sample I) together with the electron diffraction pattern taken from hundreds of Ir nanoclusters. The electron diffraction pattern of the Ir nanoclusters matches exactly that of the bulk Ir metal powder (examined back-to-back for comparison and as a control). This result indicates that the Ir nanoclusters consist of metallic Ir(0) cores in which Ir metal atoms are cubic close-packed (ccp or, equivalently, face-centered cubic, fcc), exactly as in bulk Ir(0) metal. Thus according to the average size (30 Å) and the density of bulk Ir metal (22.5 g/cm³), the Ir nanoclusters can be *represented*[29] as $Ir_{\sim 900}$. An ultracentrifugation sedimentation equilibrium solution molecular-weight measurement[30] of the Ir nanocluster provides a weight-average molecular weight, $\overline{M}_r$ = (1.8 ± 0.8) × 10^5 (Figure D, supplementary material). Note that this *solution* molecular weight is consistent within experimental error with the TEM-obtained estimate of the MW of Ir_{900} (i.e., 1.7 × 10^5 amu).

The presence of the polyoxoanion in the $Ir_{\sim 900}$ nanoclusters was independently and unequivocally demonstrated by IR, FABMS, and elemental analysis. The IR spectrum (Figure E, supplementary material) exhibits bands characteristic of the $P_2W_{15}Nb_3O_{62}^{9-}$ polyoxoanion or its well-known Nb–O–Nb bridged $P_4W_{30}Nb_6O_{123}^{16-}$ aggregate, the latter being formed from two $P_2W_{15}Nb_3O_{62}^{9-}$ aggregates by the addition of two H^+ and

(22) (a) Pope, M. T. *Heteropoly and Isopoly Oxometalates*; Springer-Verlag: New York, 1983. (b) Pope, M. T.; Müller, A. *Angew. Chem., Int. Ed. Engl.* **1991**, *30*, 34.

(23) (a) In fact, several observations made us believe initially[23b,c] that the catalytic hydrogenation of cyclohexene beginning with $(1,5\text{-}COD)Ir{\cdot}P_2W_{15}Nb_3O_{62}^{8-}$ was, rather than Ir nanocluster catalysis, catalysis by a discrete "$H_2Ir{\cdot}P_2W_{15}Nb_3O_{62}^{8-}$" complex. These observations included the homogeneous catalyst-like, ±15% reproducibility;[23d] the fact that the catalyst could be prepared in organic solvents, isolated, and then redissolved with little loss in its catalytic activity (a phenomenon virtually unheard of for colloids when we began these studies in 1982);[23d] and the lack of a more general solution to the difficult mechanistic problem of distinguishing "homogeneous" from "heterogeneous" catalysts, a problem we have a more general solution to as part of this work (reported elsewhere[24]). (b) Lyon, D. K. Ph.D. Thesis, University of Oregon, 1990. (c) Lyon, D. K.; Finke, R. G. *Inorg. Chem.* **1990**, *29*, 1787–9. (d) Another reason for the homogeneous catalyst-like reproducibility may be that a so-called "structure-insensitive" reaction, the hydrogenation of cyclohexene, was examined, something that is under further investigation (i.e. the structure-sensitive or -insensitive nature of metal nanocluster reactions).[24] (e) Edlund, D. J. Ph.D. Thesis, University of Oregon, 1987.

(24) Lin, Y.; Finke, R. G. *Inorg. Chem.*, in press.

(25) (a) Finke, R. G.; Lyon, D. K.; Nomiya, K.; Sur, S.; Mizuno, N. *Inorg. Chem.* **1990**, *29*, 1784–7. (b) Pohl, M.; Finke, R. G. *Organometallics* **1993**, *12*, 1453. (c) A full paper is under preparation: Pohl, M.; Lyon, D. K.; Mizuno, N.; Nomiya, K.; Finke, R. G. Submitted to *Inorg. Chem.* for publication.

(26) If the reaction is carried out under a lower, 1-atm pressure of H_2, the resultant Ir particles have a similar size but are less spherical (Figure 13). Under these milder conditions, no bulk Ir(0) metal particles were observed but a few floccules of the Ir nanoclusters are detected. The difference in the morphology of the Ir nanoclusters prepared at higher vs lower H_2 pressure is discussed further in the Minimum Mechanism (Discussion) section.

(27) (a) Reference 22a, pp 101–117 and references therein. (b) Pope, M. T. *Mixed-Valence Compounds*; Brown, D. B., Ed.; Reidel: Dordrecht, The Netherlands, 1980; p 365. (c) Buckley, R. I.; Clark, R. J. H. *Coord. Chem. Rev.* **1985**, *65*, 167.

(28) (a) Perez-Benito, J. F.; Arias, C. *Int. J. Chem. Kinet.* **1991**, *23*, 717. (b) Perez-Benito, J. F.; Lee, D. G. *Can. J. Chem.* **1985**, *63*, 3545. (c) Freeman, F.; Chang, L. Y.; Kappos, J. C.; Sumarta, L. *J. Org. Chem.* **1987**, *52*, 1460. (c) For a compilation of the absorption spectra of the colloidal metallic elements, see: Creighton, J. A.; Eadon, D. G. *J. Chem. Soc., Faraday Trans.* **1991**, *87*, 3881. (d) Wilcoxon, J. P.; Williamson, R. L.; Baughman, R. *J. Chem. Phys.* **1993**, *98*, 9933.

(29) (a) The number (N) of Ir atoms in a Ir nanocluster within a given diameter can be approximated using the following equation: $N = (N_0\rho V)/192.2$, where $N_0 = 6.022 \times 10^{23}$, $\rho = 22.5$ g/cm³, and $V = (4/3)\pi(D/2)^3$. (b) Accordingly, an average diameter 30.0 (±4.1)-Å nanocluster can be approximated as Ir_{900}, while diameters of 25.9 Å (i.e., 30.0 − 4.1) and 34.1 Å (i.e., 30.0 + 4.1) can be approximated as Ir_{640} and Ir_{1460}, respectively. Hence, when we say $Ir_{\sim 900}$, for example, this is largely because it is convenient and also because it gives the reader some idea of the composition of the nanocluster under discussion. We *do not* mean to imply that a monodispersed, exactly $Ir_{\sim 900}$ cluster, is the only species present.

(30) (a) Chervenka, C. H. *A Manual of Methods for the Analytical Ultracentrifuge*; Spinco Division of Beckman Instruments: Palo Alto, CA, 1969. (b) Fujita, H. *Foundations of Ultracentrifugal Analysis*; Wiley: New York, 1975; pp 308–313.

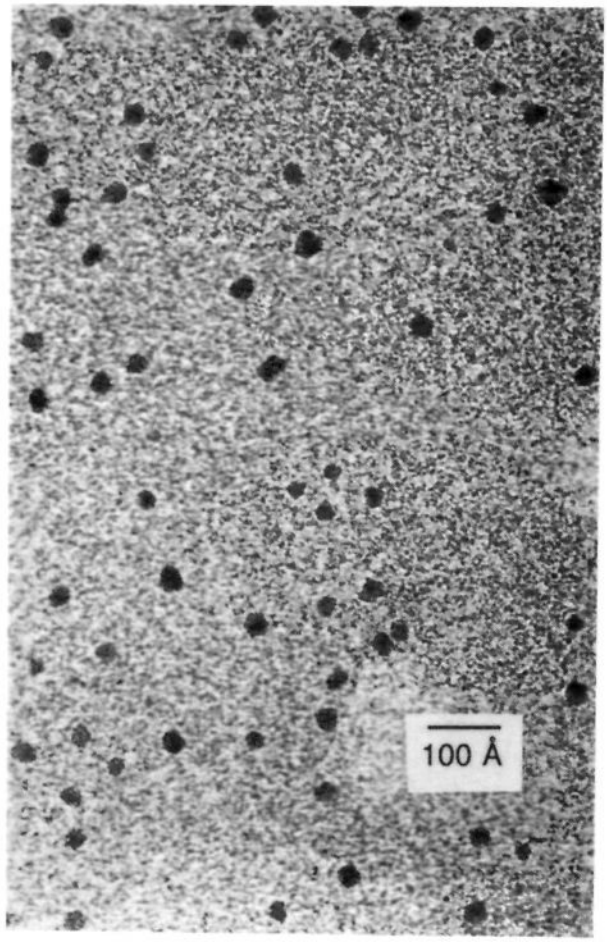

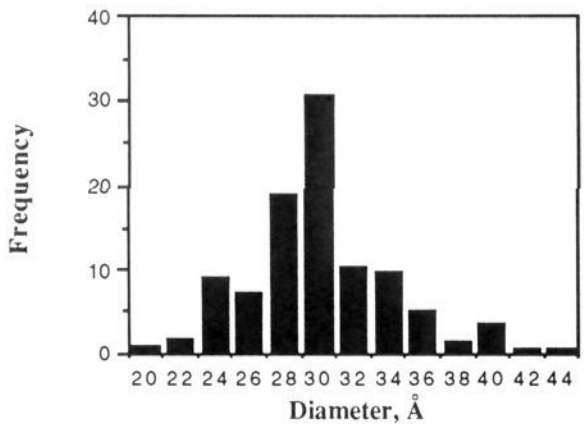

Figure 4. (A) (top) Transmission electron micrograph of the $Ir_{\sim 900}$ nanoclusters (sample I) (ca. 0.5 mg/mL of CH_3CN, spraying onto a carbon-film-coated Cu grid). The $Ir_{\sim 900}$ nanoclusters (dark spherical particles of ca. 30 Å) are well dispersed throughout the polyoxoanion matrix (small granular particles). (B) (bottom) Histogram of the Ir nanocluster diameters. The mean diameter is 30.0 Å, with a standard deviation of 4.1 Å, from a sample population of 219.

loss of H_2O.[31] Consistent with the IR studies, FAB-MS (Figure F, supplementary material) shows two peaks corresponding to $P_2W_{15}Nb_3O_{62}^{9-}$ and $P_4W_{30}Nb_6O_{123}^{16-}$, although a detailed FAB-

(31) It is very difficult to distinguish the $P_2W_{15}Nb_3O_{62}^{9-}$ monomer from the Nb–O–Nb bridged aggregate $P_4W_{30}Nb_6O_{123}^{16-}$.[31a] The aggregate has a band ca. 660 cm^{-1} but is not easily detected,[31a,b] and it appears to be somewhat sensitive to the presence of low levels of H_2O.[31b] (a) Edlund, D. J.; Saxton, R. J.; Lyon, D. K.; Finke, R. G. *Organometallics* **1988**, *7*, 1692–704. (b) Nomiya, K.; Kaneko, M.; Kasuga, N.; Finke, R. G.; Pohl, M. *Inorg. Chem.* **1994**, *33*, 1469.

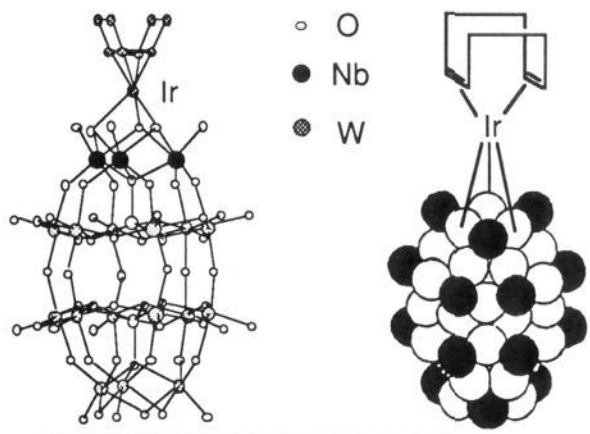

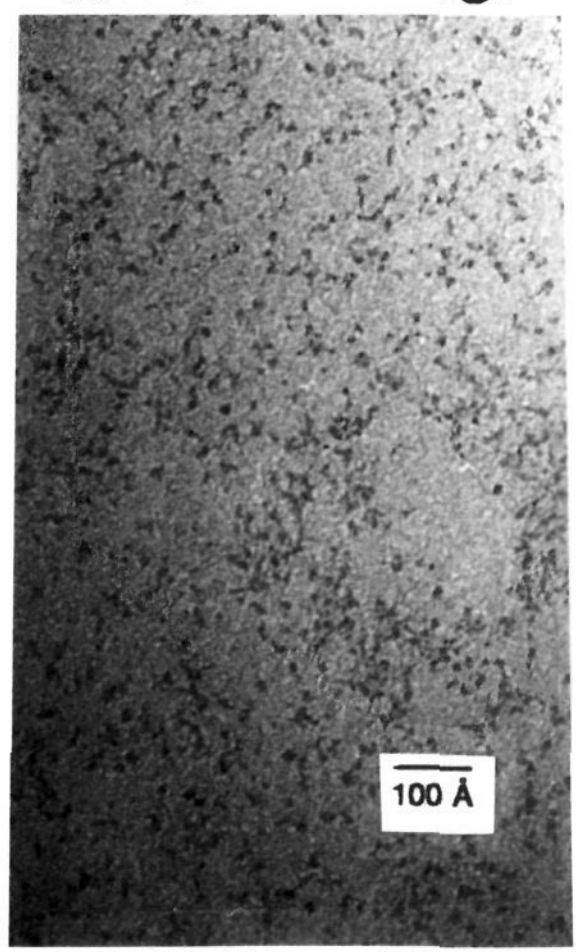

Figure 5. (A) (top) Ball and stick representation (left) of the average C_{3v} (pseudo) symmetry solution structure of[25] (1,5-COD)Ir·$P_2W_{15}Nb_3O_{62}^{8-}$ (the center-most O, Nb, and W legend is for this left-most structure). On the right is the space-filling representation, in which the black circles represent terminal oxygens and the white circles represent bridging oxygens. (B) (bottom) Transmission electron micrograph of $(Bu_4N)_5Na_3[(1,5\text{-COD})Ir{\cdot}P_2W_{15}Nb_3O_{62}]$ (0.1 mM, sprayed onto a carbon-film-coated Cu grid) as a control. The observed granular particles are the individual $(Bu_4N)_5Na_3[(1,5\text{-COD})Ir{\cdot}P_2W_{15}Nb_3O_{62}]$ molecules.

MS study present elsewhere shows that both these species have been detected in independent FAB-MS studies beginning with authentic $P_2W_{15}Nb_3O_{62}^{9-}$ or $P_4W_{30}Nb_6O_{123}^{16-}$.[32] Hence, it is unclear which polyoxoanion is really present initially and which is generated during the FAB-MS experiment. Thus, an ultracentrifugation solution molecular-weight measurement was done to address which polyoxoanion is present in solution. Four runs

(32) Trovarelli, A.; Finke, R. *Inorg. Chem.* **1993**, *32*, 6034.

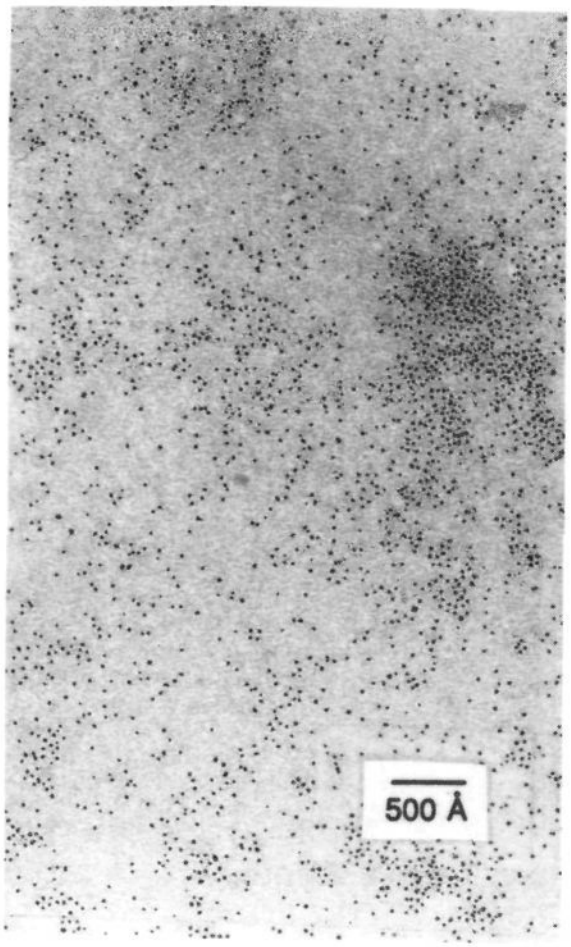

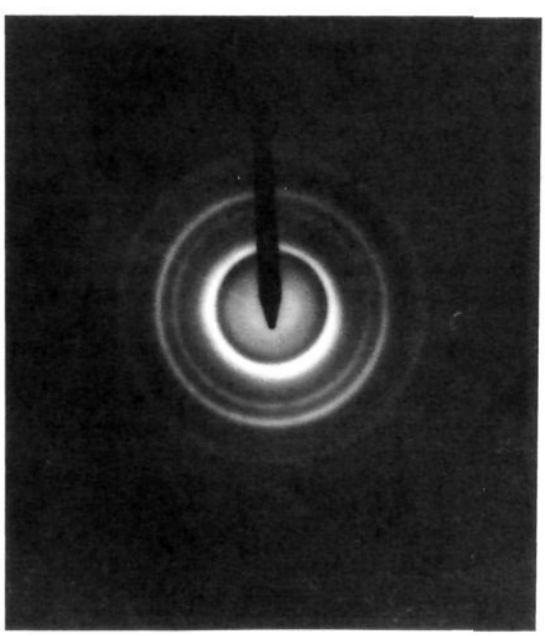

Figure 6. (A) (top) Large-area view of the $Ir_{\sim 900}$ nanoclusters demonstrating the narrow distribution of the nanocluster sizes. (B) (bottom) Electron diffraction pattern of the Ir nanoclusters. The diffraction pattern is identical to that of authentic cubic close-packed (ccp or, equivalently, face-centered cubic, fcc) Ir metal powder, examined as a control.

by two independent researchers (one run was carried out by Dr. D. Lyon[23b]) *all gave the same molecular weight (12 000 ± 2000* (Figure G, supplementary material)), indicating that the Nb–O–Nb bridged aggregate $P_4W_{30}Nb_6O_{123}^{16-}$ (FW = 8164), rather than the monomeric $P_2W_{15}Nb_3O_{62}^{9-}$ polyoxoanion (FW = 4090), is present. When combined with the elemental analysis presented in the Experimental Section, the *average* chemical composition of $Ir_{\sim 900}$ nanoclusters (sample I) can be represented in the simplest form as $Ir_{15}(P_4W_{30}Nb_6O_{123})(Bu_4N)_{11}Na_5$ or, scaling up to the $Ir_{\sim 900}$ size indicated by the TEM and solution MW measurement, $[Ir(0)_{\sim 900}(P_4W_{30}Nb_6O_{123}^{16-})_{\sim 60}](Bu_4N)_{\sim 660}Na_{\sim 300}$ [in which, *for these isolated samples*, the polyoxoanion is present in its oxidized (non-heteropolyblue) Nb–O–Nb bridged aggregate form, $P_4W_{30}Nb_6O_{123}^{16-}$]. Note that although Ir hydride formation on the nanocluster's surface is expected (e.g., based on Moiseev and co-workers'[17c] work, and under our reducing, H_2 atmosphere reaction conditions), the results presented in the next section indicate that Ir surface hydrides *are not present* at a detectable level even in solution for these $Ir_{\sim 900}$ nanoclusters.

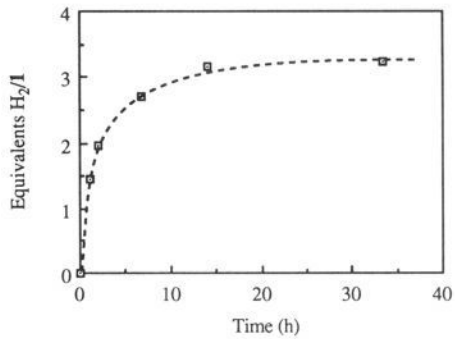

Figure 7. Uptake of 3.5 ± 0.3 equiv of H_2 per 1 equiv of $(Bu_4N)_5Na_3[(1,5\text{-COD})Ir\cdot P_2W_{15}Nb_3O_{62}]$ in acetone at 22 °C.

Scheme 1. Rationalization of the 3.5 Equiv of H_2 Uptake per 1 Equiv of $(Bu_4N)_5Na_3[(COD)Ir\cdot P_2W_{15}Nb_3O_{62}]$

$$(1,5\text{-COD})Ir^{I}\cdot P_2W_{15}Nb_3O_{62}^{8-} + 2.5\ H_2 \longrightarrow$$

(1,5-COD = ⬡)

$$Ir(0) + \text{⬡} + H^+ + P_2W_{15}Nb_3O_{62}^{9-} \quad (1)$$

$$(n\rightarrow m)\ Ir(0) \longrightarrow Ir(0)_{n\rightarrow m} \quad (2)$$

$$P_2W_{15}Nb_3O_{62}^{9-} + H^+ \longrightarrow 0.5\ P_4W_{30}Nb_6O_{123}^{16-} + 0.5\ H_2O \quad (3)$$

$$0.5\ P_4W^{VI}{}_{30}Nb_6O_{123}^{16-} + H_2 \xrightarrow[\text{catalysis}]{Ir(0)_{n\rightarrow m}} 0.5\ P_4W^{VI}{}_{26}W_4{}^{V}Nb_6O_{123}^{20-} + 2\ H^+ \quad (4)$$

(heteropolyblue)

Hydrogen Uptake Stoichiometry and the Formation of the Polyoxoanion "Heteropolyblue".[27] To see if we could further define the Ir nanocluster's (average) stoichiometry, quantitative H_2 uptake experiments were performed (note, however, that these are <1 atm H_2 of experiments whereas the previous $Ir_{\sim 900}$ nanoclusters were prepared at 40 psig (i.e., at 2.7 atm) of H_2).[33] Under a H_2 pressure of 250 mmHg, $(Bu_4N)_5Na_3[(1,5\text{-COD})Ir\cdot P_2W_{15}Nb_3O_{62}]$ (8.81 mM in acetone) smoothly consumed 3.5 ± 0.3 equiv of H_2 at 22 °C (Figure 7) and released 1.0 ± 0.1 equiv of cyclooctane (by GC and ^1H NMR). During the hydrogen uptake experiment, the original clear-yellow solution turns blue, but this blue color is lost over ca. 5 min in a N_2 drybox (containing <1 ppm of O_2) after the H_2 atmosphere is released. Solution molecular-weight measurements of the product solution (at 20 000 rpm and monitoring at 360 nm) gave a molecular weight twice that of $P_2W_{15}Nb_3O_{62}^{9-}$, indicating that the $P_2W_{15}Nb_3O_{62}^{9-}$ polyoxoanions have again formed the known Nb–O–Nb aggregate,[31] $P_4W_{30}Nb_6O_{123}^{16-}$.

The H_2 uptake stoichiometry, the formation of the blue color, and the presence of the Nb–O–Nb bridged polyoxoanion aggregate are rationalized in Scheme 1. The release of 1.0 equiv of 1,5-cyclooctadiene as reduced cyclooctane and the formation

(33) Reference 23b, pp 61–62, 89–90.

of Ir(0) require that each $(Bu_4N)_5Na_3[(1,5\text{-COD})Ir{\cdot}P_2W_{15}Nb_3O_{62}]$ consumes 2.0 equiv of H_2 for the reduction of cyclooctadiene to cyclooctane and 0.5 equiv of H_2 for the reduction of Ir(I) to Ir(0) (step 1, Scheme 1). Oxidative titration and appropriate control experiments demonstrate that the remaining 1.0 equiv of H_2 is consumed by 0.5 equiv of $P_4W_{30}Nb_6O_{123}^{16-}$ (formed[31] by aggregation of two $P_2W_{15}Nb_3O_{62}^{9-}$ complexes in the presence of H^+ (step 3)) to give 0.5 equiv of the 4e⁻-reduced, W^V-containing heteropolyblue, $P_4W^{V}_{26}W^{V}_4Nb_6O_{123}^{20-}$ (step 4). (Control experiments also show that $P_4W_{30}Nb_6O_{123}^{16-}$ is readily reduced by H_2 to heteropolyblue in the presence of an authentic $Ir(0)/Al_2O_3$ catalyst.) Thus the formation of the heteropolyblue most likely occurs via chemisorption of H_2 onto the Ir(0) surface and then its "spillover" to the polyoxoanion. Note that the 3.5 equiv of H_2 uptake stoichiometry, plus the product studies (including the formation of 0.5 equiv of a 4e⁻-reduced heteropolyblue), means that precedented species such as hydrido nanoclusters,[17c] $Ir(0)_xH_n$, or, equivalently, reduced nanoclusters with surface protons, $(Ir)_x^{n-}(H)_n^{n+}$, *are not present* (at least not in the present nanocluster sample which includes the mildly oxidizing polyoxoanion). *This is the first case, despite the extensive literature of metal colloids, where the presence of such surface hydrides has been unequivocally ruled out.* Note, however, that the presence of the somewhat oxidizing polyoxoanion, which effectively can "clean" the Ir nanocluster's surface of $H^\bullet$ or H^- reducing equivalents, might mean that this finding may not be more generally applicable to other nanoclusters and colloids.

On the other hand, the observation of H_2 reducing equivalents (in this case as $H^+ + e^-$) "spilling over" onto the soluble polyoxoanion metal oxide provides a molecular version of the well-known, commercially important, but poorly understood "spillover"[34] of H_2 (as either $H^\bullet$ or H^+/e^-; which occurs is controversial).[34a,b,c] Hence this system also provides the first molecular model of H_2 spillover, one where spillover occurs as an e^- (reduced W^V) and H^+. This system would appear, therefore, to be worthy of further investigation (additional studies of this spillover model are planned).

Stabilization of the ca. 30-Å $Ir_{\sim 900}$ Nanoclusters: Is This Achieved by the Adsorption of Polyoxoanions onto the $Ir_{\sim 900}$ Nanocluster Surface? The $Ir_{\sim 900}$ nanoclusters in acetone or acetonitrile solution are quite stable: no bulk Ir(0) precipitate is found after more than 3 months at room temperature in a ≤1.0 ppm of O_2 drybox (although heating at 50 °C for 2 days causes the Ir nanoclusters to precipitate from solution as a result of aggregation at elevated temperature, as expected). This raises the important question of how are the $Ir_{\sim 900}$ nanoclusters stabilized against further aggregation and against the formation of bulk Ir metal particles? Since no "steric stabilizing" polymer is added, the stability of the $Ir_{\sim 900}$ nanocluster must be due to charge stabilization (i.e., via electrostatic repulsion). The charge to the nanoclusters and colloids is generally acquired by the adsorption of ions (for example Cl^- is a typical *mono*anion);[35] the negative polyoxoanion and its associated cationic Bu_4N^+ are the only possible sources of such charge stabilization in the present case.

To determine whether the $Ir_{\sim 900}$ nanoclusters are stabilized by surface adsorption of (negative) polyoxoanions or (cationic) Bu_4N^+, an electrophoresis experiment was conducted. It is found that, under a 24.5-V electric field, the $Ir_{\sim 900}$ nanoclusters migrate steadily toward the *positive* electrode at a speed of 9 mm/h (as measured by the displacement of the boundary formed between the amber acetonitrile solution of $Ir_{\sim 900}$ nanoclusters and the 2 mM $(Bu_4N)^+(PF_6)^-/CH_3CN$ electrolyte solution; the same result is also obtained when pure CH_3CN solvent was used to replace the 2 mM $(Bu_4N)^+(PF_6)^-/CH_3CN$ electrolyte solution). *These results indicate unambiguously that the $Ir_{\sim 900}$ nanoclusters are negatively charged*; this in turn demands that the nanocluster surface contains predominately polyoxoanions (and that the associated Bu_4N^+ countercations, plus additional polyoxoanions, be primarily in the outer, electrical double or diffusion layer common in "colloids", recall Figure 1a).[35] According to the migration velocity and the field strength, the electrophoretic mobility[36] (μ_E) of the $Ir_{\sim 900}$ nanoclusters can be calculated to be 2.5×10^{-4} cm²/V s. This value is similar to those reported for a variety of small particles in nonaqueous solution (e.g., 1.7×10^{-4} cm²/V s for ca. 80-Å palladium in acetone),[14e] as well as in aqueous solution (e.g., 2×10^{-4} cm²/V s for ca. 1000-Å platinum and $3–4 \times 10^{-4}$ cm²/V s for ca. 1000-Å gold).[37] Although it is impossible to determine the exact number of negative charges on each nanocluster from the electrophoretic mobility, the potential at the surface of the $Ir_{\sim 900}$ nanoclusters (the ζ potential) can be approximated using Hückel's equation[38,39] to be –40 mV,[40] a value comparable to that of ca. 80-Å palladium in acetone solution, –44 mV.[14e]

Additional, independent evidence supporting the finding that the $Ir_{\sim 900}$ nanoclusters are negatively charged was obtained from experiments using ion-exchange resins. The amber acetone solution of $Ir_{\sim 900}$ nanoclusters readily passed down a *cation*-exchange column (Amberlite IRA-400 resin) in the Bu_4N^+ form ($P\text{–}SO_3^-Bu_4N^+$, P = macroreticular polymer) without a change in the color, and unchanged ca. 30-Å Ir nanoclusters were visualized by TEM in the collected, amber column effluent (a result which further demonstrates the stability of these $Ir_{\sim 900}$ nanoclusters). When the amber solution of $Ir_{\sim 900}$ nanoclusters was loaded and passed down an *anion*-exchange column (Amberlyst A-27) in either the Cl^- form or the BF_4^- form ($P\text{–}NR_3^+$-Cl^- or BF_4^-, P = macroreticular polymer), a colorless column effluent was collected, and TEM showed no Ir nanoclusters or bulk Ir metal particles in the effluent. These results indicate that the $Ir_{\sim 900}$ nanoclusters are adsorbed to the anion-exchange resin (i.e., to $P\text{–}NR_3^+$) but not to the cation-exchange resin (i.e., not to $P\text{–}SO_3^-$), which in turn confirms that the $Ir_{\sim 900}$ nanoclusters are negatively charged.[41]

The attachment of the polyoxoanions to the $Ir_{\sim 900}$ nanocluster surface, thereby kinetically stabilizing the $Ir_{\sim 900}$ nanoclusters against aggregation and formation of bulk Ir metal particles, is further supported by the following isolation and TEM experiment. When ether was added to an acetone solution of the $Ir_{\sim 900}$ nanoclusters and the resultant cloudy solution was centrifuged at 14 000 rpm for 10 min, a cloudy light-amber supernatant and a dark-brown precipitate were obtained. TEM showed that the light-amber supernatant contained a small amount of ca. 30-Å Ir particles well dispersed in the polyoxoanion matrix (Figure

(34) (a) Bond, G. C. In *Studies in Surface Science and Catalysis*; Pajonk, G. M., Teichner, S. J., Germain, J. E., Eds.; Elsevier: Amsterdam, 1982; Vol. 17, p 1. (b) Berznis, A. R.; Sermon, P. A. *Nature* **1983**, *303*, 506. (c) Sermon, P. A.; Bond, G. C. *Catal. Rev. 1973*, *8*, 211. (d) The significance of $H^\bullet$ spillover is attested to by the following quotes from one of the better reviews on spillover: [34a] "Spillover... is a phenomenon of wide if not universal occurrence with supported catalysts, and one of the least well understood effects. Its importance cannot be overstated". Another quote[34a] is the following: "It is quite possible, indeed likely, that much of the now puzzling information on support effects in metal catalysis will ultimately be resolved by the application of spillover concepts."

(35) Shaw, D. J. *Introduction to Colloid and Surface Chemistry*, 4th ed.; Butterworths-Heinemann: Boston, MA, 1992; pp 174–176.

(36) μ_E = (velocity)/(field strength) = (0.9 cm/3600 s)/(–24.5 V/25.0 cm) = 2.5×10^{-4} cm²/V s.

(37) Jirgensons, B.; Straumanis, M. E. *Colloid Chemistry*, 2nd ed.; Macmillan: New York, 1962; p 132.

(38) Shaw, D. J. *Electrophoresis*; Academic: New York, 1969; pp 15–21.

(39) Hunter, R. J. *Zeta Potential in Colloid Sciences*; Ottewill, R. H., Rowell, R. L., Eds.; Academic: New York, 1981; p 69.

(40) According to Hückel's equation,[38,39] $\zeta = (3/2)\mu_E\eta/(\epsilon_0 D)$, where D is the dielectric constant (37.5 for acetonitrile), ϵ_0 is the permittivity (8.854×10^{-12} F/m), and η is the solvent viscosity (3.4×10^{-4} N s/m² for acetonitrile).

(41) For relevant work, on the adsorption of surfactant-stabilized (i.e., charged-stabilized) noble metal colloids onto ion-exchange resins, see: Nakao, Y.; Kaeriyama, K. *J. Colloid Interface Sci.* **1989**, *131*, 186–91.

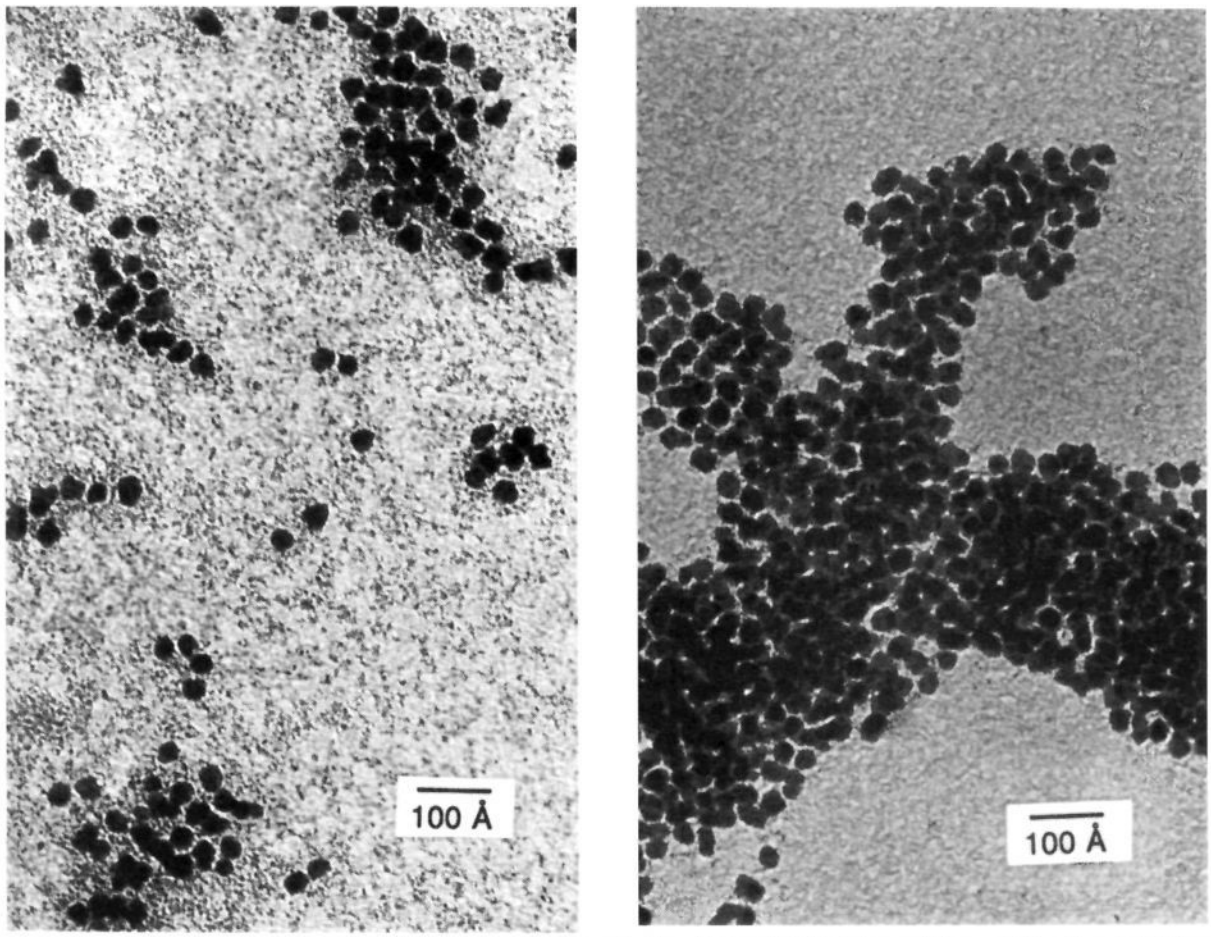

Figure 8. Transmission electron micrographs of the $Ir_{\sim 900}$ nanoclusters, after the addition of diethyl ether and then centrifugation at 14 000 rpm, a procedure which removes some of the nanocluster-stabilizing polyoxoanion. (A) (left) Transmission electron micrograph of the *supernatant* showing the discrete Ir nanoclusters dispersed in the polyoxoanion matrix. (B) (right) Transmission electron micrograph of the *precipitate* (redispersed in CH_3CN and then sprayed onto a carbon-film-coated Cu grid), showing floccules of Ir nanocluster aggregates and very few polyoxoanions.

8a). However, the dark-brown precipitate (redispersed into acetonitrile for TEM studies) contained primarily large *aggregated floccules* consisting of ca. 30-Å Ir particles, *with fewer polyoxoanions* being found nearby (Figure 8b). This observation demonstrates, therefore, that the polyoxoanions are necessary to stabilize the ca. 30-Å Ir particles and to keep them well dispersed. Further information about the interaction between the polyoxoanions and the ca. 30-Å Ir particles may be possible using EXAFS or HRTEM (high-resolution TEM), experiments which are under investigation.

It is worth noting here that all the polyoxoanion $P_2W_{15}Nb_3O_{62}^{9-}$ and $(Bu_4N^+)_9^{9+}$ stabilization of the nanocluster seen herein is of a novel if not unprecedented type—a combined, *very high* charge and *large* size stabilization built in *intrinsically* to the (large) polyoxoanion^{9-} and (large) nine Bu_4N^+ combination—especially when one realizes that the size of *nine* Bu_4N^+ molecules is larger than one tends to realize initially. (A comparison makes this point about combined charge and size stabilization clearer. A typical literature colloid provides *independent* charge and steric bulk stabilization—for instance, charge stabilization by Cl^- and steric bulk stabilization by an added polymer.) Also, the diffuse double (or really multi-) layer composed of the polyoxoanions and Bu_4N^+ cations should be relatively thick and, therefore, should provide a high degree of stabilization for the nanocluster (although the *inverse* dependence of the thickness of the multilayer upon change needs to be noted here[35]). Further studies of other X^-, polyanionic^{n-} ligands and different, even bulkier, alkyl R_4N^+ are planned to test more rigorously this preliminary conclusion about the origins of this enhanced nanocluster stability.

In Situ Generation of Smaller 20 ± 3 Å $Ir_{\sim 300}$ Nanoclusters (Sample II) from $(Bu_4N)_5Na_3[(1,5\text{-COD})Ir{\cdot}P_2W_{15}Nb_3O_{62}]$ and 23 ± 3 Å $Ir_{\sim 400}$ Nanoclusters (Sample III) from $(Bu_4N)_4Na_2[(1,5\text{-COD})Ir{\cdot}SiW_9Nb_3O_{40}]$ during the Catalytic Hydrogenation of Cyclohexene in Acetone. As mentioned earlier, the present polyoxoanion-dispersed nanoclusters were first uncovered following extensive mechanistic studies (presented elsewhere)[24] of the hydrogenation of cyclohexene beginning with $(Bu_4N)_5Na_3[(1,5\text{-COD})Ir{\cdot}P_2W_{15}Nb_3O_{62}]$ or with a second polyoxoanion-supported $Ir(1,5\text{-COD})^+$ species that we have prepared,[42] $(Bu_4N)_4Na_2[(1,5\text{-COD})Ir{\cdot}SiW_9Nb_3O_{40}]$. Hence, it is important to characterize these nanoclusters as well (eqs 5–7).

$$(1,5\text{-COD})Ir{\cdot}P_2W_{15}Nb_3O_{62}^{8-} + 3.5\ H_2 \longrightarrow (1/\sim 300)\ Ir_{\sim 300}{\cdot}\text{polyoxoanion nanoclusters}) + \bigcirc \quad (5)$$

$$(1,5\text{-COD})Ir{\cdot}SiW_9Nb_3O_{40}^{6-} + 2.5\ H_2 \longrightarrow (1/\sim 400)\ Ir_{\sim 400}{\cdot}\text{polyoxoanion nanoclusters}) + \bigcirc \quad (6)$$

$$\bigcirc + H_2 \xrightarrow{Ir_{\sim 300}\text{ or }Ir_{\sim 400}\ \cdot\text{polyoxoanion nanoclusters}} \bigcirc \quad (7)$$

As described in more detail elsewhere,[24] the clear-yellow solution of 1.0 mM $(Bu_4N)_5Na_3[(1,5\text{-COD})Ir{\cdot}P_2W_{15}Nb_3O_{62}]$ in Burdick and Jackson acetone at 40 psig of H_2 and in the presence of 1.65 M purified cyclohexene evolves into an active catalyst after an induction period of 2.0 ± 0.2 h. The Ir nanoclusters

(42) Lin, Y.; Nomiya, K.; Finke, R. G. *Inorg. Chem.* **1993**, *32*, 6040.

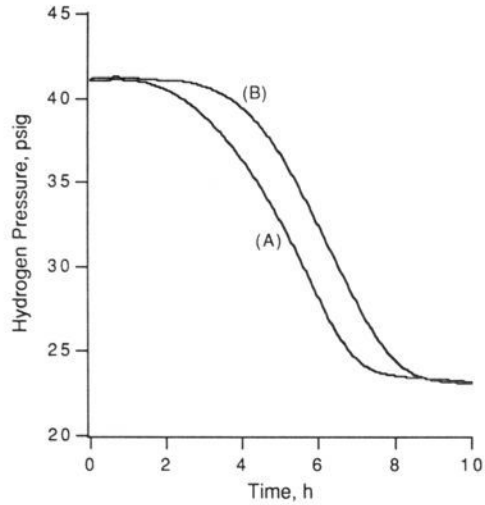

Figure 9. Typical reaction progress curve for cyclohexene hydrogenation starting with (A) 1.2 mM $(Bu_4N)_5Na_3[(1,5\text{-COD})Ir{\cdot}P_2W_{15}Nb_3O_{62}]$, or (B) $(Bu_4N)_4Na_2[(1,5\text{-COD})Ir{\cdot}SiW_9Nb_3O_{40}]$, plus 1.65 M cyclohexene in acetone and 40 psig of H_2.

(sample II), that are slowly generated in situ, then catalyze the cyclohexene hydrogenation over 8 h (Figure 9). (Note that the H_2 uptake needed for the generation of Ir nanoclusters and the heteropolyblue is negligible compared with that required by cyclohexene hydrogenation.) The originally yellow solution slowly turns turbid-amber and then finally deep-blue (again due to heteropolyblue formation) once ca. 90% of the cyclohexene has been converted to cyclohexane. A blue filtrate and a small amount of brown precipitate were obtained by filtering the cloudy product mixture through No. 2 Whatman paper in an inert atmosphere drybox. The brown precipitate is soluble in acetone (and very soluble in acetonitrile), giving an amber solution. TEM (Figure 10) shows that the amber solution contains 20.3 ± 2.8 Å (i.e., ±14%) Ir nanoclusters ($Ir_{\sim 300}$, sample II)[43a,29] together with polyoxoanions, while the filtrate contains significantly fewer, yet similarly sized, Ir nanoclusters (Figure H, supplementary material). These results indicate that most of the Ir nanoclusters are in the precipitate, apparently precipitated by the cyclohexane formed as the hydrogenation of cyclohexene proceeds. In addition, TEM shows that the precipitation process has no observable effect on the Ir nanocluster size. When compared to the 30 ± 4 Å $Ir_{\sim 900}$ nanoclusters (sample I) prepared from the H_2 reduction of $(Bu_4N)_5Na_3[(1,5\text{-COD})Ir{\cdot}P_2W_{15}Nb_3O_{62}]$, the 20 ± 3 Å $Ir_{\sim 300}$ nanoclusters made in the presence of cyclohexene/cyclohexane are ca. 30% smaller, presumably due to a slower growth rate [perhaps due to the competitive adsorption of cyclohexene on the metal cluster's surface or, conceivably, due to some other aspect of the nanocluster formation mechanism, *vide infra*].

(43) (a) Actually, 20 ± 3 Å corresponds to $Ir_{450-190}$, while the average diameter of 20 Å corresponds to $Ir_{\sim 300}$.[29] (b) A simple, *zeroth-order* physical model for the *maximum* number of polyoxoanions that might be expected to bind onto the Ir nanoclusters' surface, and as a function of nanocluster size, was constructed as follows. First, one can calculate the surface area of ca. 20 Å $Ir_{\sim 300}$ and 30 Å $Ir_{\sim 900}$ nanoclusters, respectively, as $4\pi(20/2)^2 = 1256$ Å^2 and $4\pi(30/2)^2 = 2827$ Å^2. Then, one can calculate the maximum number of nanocluster-surface-bound polyoxoanions as follows. First it is assumed that the ca. 12 Å diameter basic Nb_3O_6 end of the $P_2W_{15}Nb_3$ polyoxoanion coordinates to the Ir nanocluster surface in a Ir-metal matching, *cubic-close packed* (*ccp*) *way* (which is, again, certainly an upper limit on the true number of polyoxoanion that could possibly coordinate). Next, given that the surface of a unit cell of ccp 12 Å species contains two Nb_3O_6 polyoxoanion ends in a 12 Å × 12 Å unit cell (i.e., 144/2 or 72 Å^2 per Nb_3O_6 polyoxoanion end; see Figure 4.1e on p 120 in Well's text[17f]), it is readily calculated that, for the $Ir_{\sim 300}$ nanocluster, up to 1256 Å^2/72 A^2 or 17 polyoxoanions could coordinate to the surface (33 or ca. twice this are found by analysis; probably only 1/3 of these are surface-coordinated at any one time). For the $Ir_{\sim 900}$ nanocluster, an analogous calculation yields 2827 Å^2/72 Å^2 or 39 polyoxoanions (in comparison to the ca. 60 found by analysis). Therefore, the calculated (and found) Ir to polyoxoanion ratios are 17:1 (found = 9:1) for $Ir_{\sim 300}$ and 23:1 (found 15:1) for $Ir_{\sim 900}$.

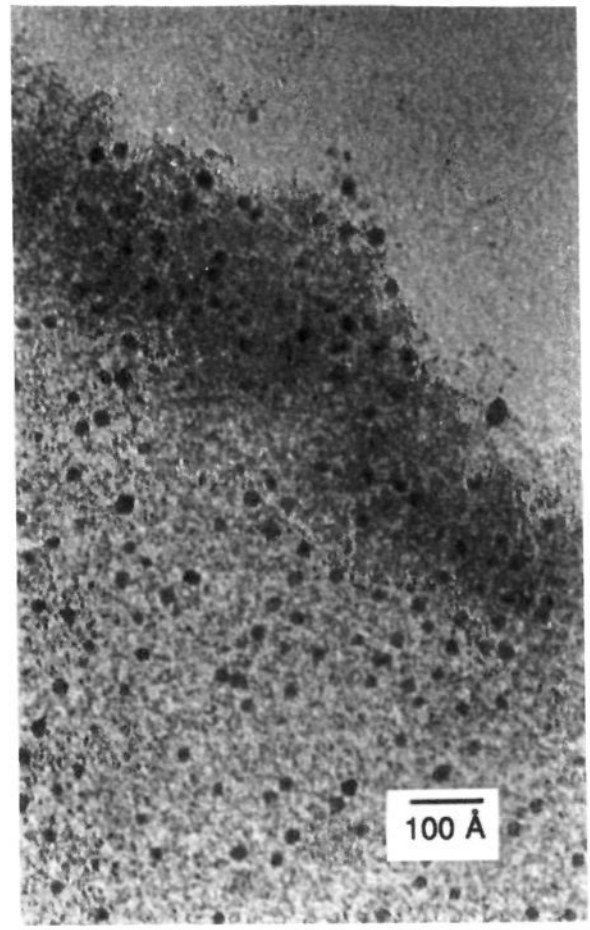

Figure 10. (A) (top) Transmission electron micrograph of the $Ir_{\sim 300}$ nanoclusters prepared from the reaction of $(Bu_4N)_5Na_3[(1,5\text{-COD})Ir{\cdot}P_2W_{15}Nb_3O_{62}]$ with H_2 in the presence of cyclohexene. The Ir nanoclusters (dark spherical particles of ca. 20 Å) are well dispersed in the polyoxoanion matrix (small granular particles). The top and rightmost corner shows the TEM image of the carbon-film background. (B) (bottom) Histogram of the Ir nanocluster diameters. The mean diameter is 20.3 Å, with a standard deviation of 2.8 Å, from a sample population of 366.

The amber solution containing the 20 ± 3 Å $Ir_{\sim 300}$ nanoclusters was further characterized by optical spectroscopy and solution molecular-weight measurements. The optical spectrum in the visible range showed a trailing decrease in adsorption with increasing wavelength (Figure I, supplementary material) similar to that of 30 ± 4 Å $Ir_{\sim 900}$ nanoclusters. Solution molecular-weight measurements (Figures J and K) indicate that the polyoxoanion is again present in its Nb–O–Nb aggregate form

(i.e., $P_4W_{30}Nb_6O_{123}^{16-}$) instead of its monomeric form (i.e., $P_2W_{15}Nb_3O_{62}^{9-}$), and the average molecular weight of the Ir nanoclusters, $(8.6 \pm 4.0) \times 10^4$, matches the range expected for the TEM-determined average of 20-Å, $Ir_{\sim 300}$ nanoclusters (i.e., 5.7×10^4). Isolation and further characterization studies, presented elsewhere,[24] establish the *average* chemical composition of the $Ir_{\sim 300}$ nanoclusters as $[Ir(0)_{\sim 300}(P_4W_{30}Nb_6O_{123}^{16-})_{\sim 33}]$-$(Bu_4N)_{\sim 300}Na_{\sim 233}$.

Note that the Ir to polyoxoanion ratio of 9:1 in the $Ir_{\sim 300}(P_4W_{30}Nb_6O_{123}^{16-})_{\sim 33}$ sample is smaller than the 15:1 value seen for the larger $Ir_{\sim 900}(P_4W_{30}Nb_6O_{123}^{16-})_{\sim 60}$ nanoclusters. This is as expected if the polyoxoanions bind to the nanocluster surface, since the smaller $Ir_{\sim 300}$ has a greater fraction (ca. 52%) of its Ir atoms on its surface than does $Ir_{\sim 900}$ (39%), a point readily verified by calculating the number of Ir atoms on the surface of idealized Ir_{309} and Ir_{923} "*magic number*" clusters.[17] *Moreover, a simple* geometrical model of adsorption of the $P_2W_{15}Nb_3O_{62}^{9-}$ onto the nanoclusters' surface, plus a back-of-the-envelope calculation,[43b] predicts Ir:polyoxoanion ratios of 17:1 (for $Ir_{\sim 300}$) and 23:1 (for $Ir_{\sim 900}$), the trend of which at least mirrors the observed ratios of 9:1 and 15:1. Hence, the elemental analysis of the isolated clusters is the fourth piece of evidence revealing that the polyoxoanions bind to the nanocluster's surface. (The other three types of evidence are the electrophoresis experiments, the ion-exchange resin tests, and the TEM studies demonstrating that the nanoclusters aggregate following removal of some of the polyoxoanions using diethyl ether).

The cyclohexene hydrogenation reaction and resultant $Ir_{\sim 400}$ nanoclusters using 1 mM $SiW_9Nb_3O_{40}^{7-}$-supported $Ir(1,5\text{-COD})^+$ complex $(Bu_4N)_4Na_2[(1,5\text{-COD})Ir{\cdot}SiW_9Nb_3O_{40}]$ (plus 40 psig of H_2 and 1.65 M cyclohexene in Burdick and Jackson acetone) parallel the results obtained above using $(Bu_4N)_5Na_3[(1,5\text{-COD})Ir{\cdot}P_2W_{15}Nb_3O_{62}]$. The active cyclohexene hydrogenation catalyst ($Ir_{\sim 400}$ nanoclusters (sample III)) evolves after an induction period of 2.5 ± 0.3 h (Figure 9). During the reaction, the originally clear-yellow solution gradually turns into turbid-amber but no heteropolyblue is observed (presumably due to the more negative ca. −1.6 V vs SCE reduction potential of the $SiW_9Nb_3O_{40}^{7-}$ polyoxoanion).[44] TEM (Figure 11) shows the presence of 23 ± 3 Å $Ir_{\sim 400}$ nanoclusters (actually $Ir_{\sim 270\text{-}640}$)[29] in the turbid-amber product solution. The average size of these Ir nanoclusters is the same as that of the 20 ± 3 Å Ir nanoclusters (sample II) within experimental error.

Control Experiment Consisting of the *in Situ* Generation of Polyoxoanion-Free 14 ± 4 Å $Ir_{\sim 100}$ Nanoclusters (Sample IV) from $[(1,5\text{-COD})Ir{\cdot}(acetone)_2]BF_4$ plus 2 Equiv of Bu_4NOH during the Catalytic Hydrogenation of Cyclohexene in Acetone. One alternative hypothesis that occurred to us is that the (quite basic) $P_2W_{15}Nb_3O_{62}^{9-}$ and $SiW_9Nb_3O_{40}^{7-}$ polyoxoanions might serve primarily as nothing more than "fancy" Bronsted bases. To test this possibility, the hydrogenation of cyclohexene and concomitant nanocluster formation was studied using polyoxoanion-free $[(1,5\text{-COD})Ir(acetone)_2]BF_4$ as a catalyst precursor in the presence of 0, 1, and 2 equiv of Bu_4NOH (i.e., three independent experiments).

The hydrogenation of cyclohexene starting with $[Ir(1,5\text{-COD})(acetone)_2]^+$ but *0* equiv of *Bu_4NOH* proceeds without an induction period and *produces bulk Ir metal* (as completely insoluble, black particles). With the addition of 1.0 equiv of $Bu_4N^+OH^-$, the reaction rate is slower but a deposit of bulk Ir metal is still observed. With the addition of 2 equiv of $Bu_4N^+OH^-$, the reaction rate is further slowed down and relatively stable *but nonisolable* Ir nanoclusters (sample IV) are obtained. TEM (Figure 12), shows that the resultant Ir nanoclusters, 14 ± 4 Å $Ir_{\sim 100}$ (actually $Ir_{\sim 50\text{-}200}$)[29] nanoclusters, are smaller and not quite as uniform in size (±28%) as the 20–23 Å (±14%) Ir nanoclusters described above from Ir·polyoxoanion catalyst precursors. The formation of these $Ir_{\sim 100}$ nanoclusters is presumably due to the greatly slowed rate of Ir(0) atom formation in the presence of the 2 equiv of $Bu_4N^+OH^-$ (see the hydrogen uptake vs time curve (Figure L, supplementary material)).

While it is clear that OH^- provides some of the beneficial effects exhibited by the polyoxoanions, and although the control studies with OH^- further demonstrate that the nanocluster formation reaction is under kinetic control, the hydrogenation of cyclohexene starting from $[(1,5\text{-COD})Ir(acetone)_2]BF_4$ plus 2.0

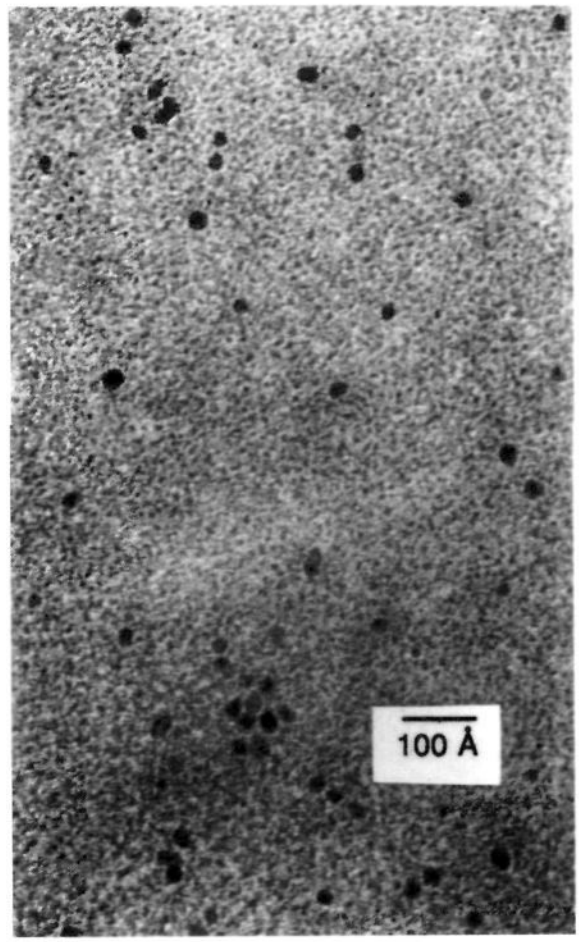

Figure 11. (A) (top) Transmission electron micrograph of the $Ir_{\sim 400}$ nanoclusters (sample III) prepared from the reaction of $(Bu_4N)_4Na_2[(1,5\text{-COD})Ir{\cdot}SiW_9Nb_3O_{40}]$ with H_2 in the presence of cyclohexene. The Ir nanoclusters (dark spherical particles of ca. 23 Å) are well dispersed in the polyoxoanion matrix (small granular particles). (B) (bottom) Histogram of the Ir nanocluster diameters. The mean diameter is 22.6 Å, with a standard deviation of 3.3 Å, from a sample population of 300.

(44) (a) Droege, M. W. Ph.D. Thesis, University or Oregon, 1984, p 138. (b) However, if formed, the 3 Nb–O–Nb bridged aggregate, $Si_2W_{18}Nb_6O_{77}^{8-}$, has a 1 V less negative −0.6 V vs SCE reduction potential in comparison to its parent $SiW_9Nb_6O_{40}^{7-}$ complex.[44a]

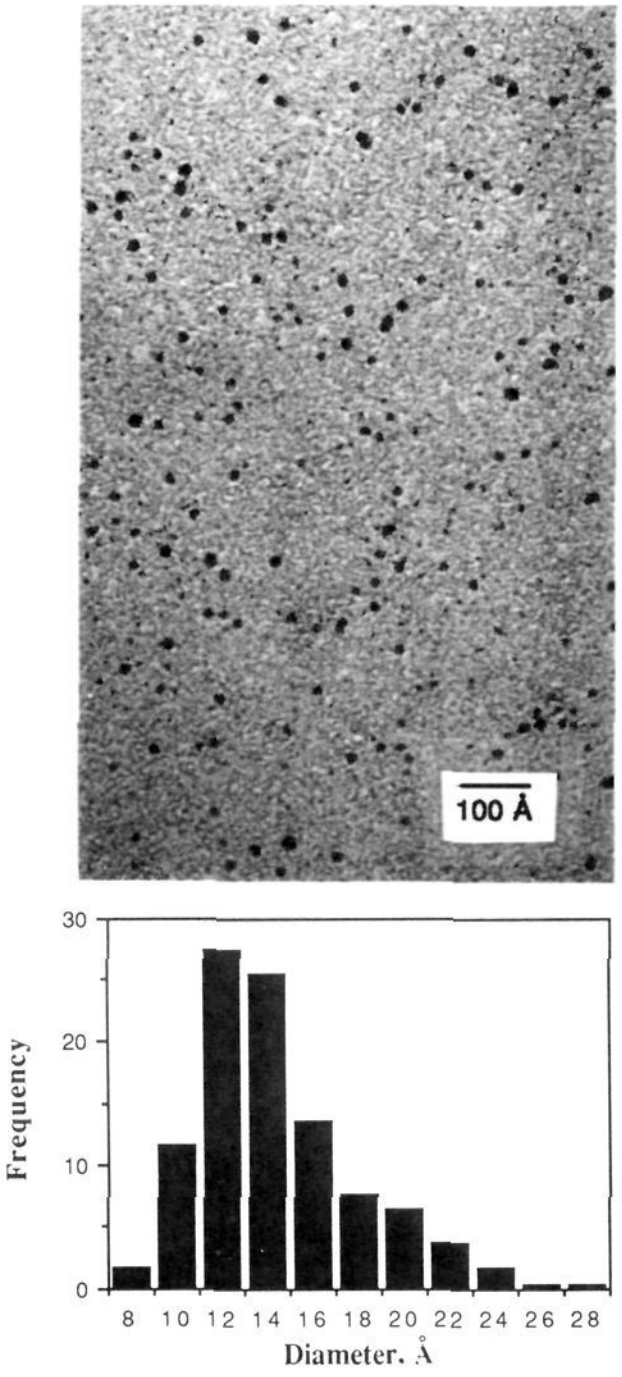

Figure 12. (A) (top) Transmission electron micrograph of the $Ir_{\sim 100}$ nanoclusters (sample IV) produced in the cyclohexene hydrogenation starting with $[(1,5\text{-COD})Ir\cdot(acetone)_2]BF_4$ plus 2 equiv of $Bu_4N^+OH^-$. (B) (bottom) Histogram of the Ir nanocluster diameters. The mean diameter is 14.4 Å, with a standard deviation of 3.6 Å, from a sample population of 340.

equiv of $Bu_4N^+OH^-$ is much different than the (1,5-COD)-Ir·polyoxoanion reactions in two key respects. These are (i) the $[(1,5\text{-COD})Ir(acetone)_2]BF_4$ plus $Bu_4N^+OH^-$ reaction is irreproducible, with unpredictable induction periods (from 0–2 h) and variable reaction rates (from 10–40 h for the completion of cyclohexene hydrogenation), and (ii) the OH^--stabilized nanoclusters are not isolable by cyclohexane addition. The similarities between $Bu_4N^+OH^-$ and the Bu_4N^+ polyoxoanions $(Bu_4N)_9P_2W_{15}Nb_3O_{62}$ and $(Bu_4N)_7SiW_9Nb_3O_{40}$ are, therefore, limited to the finding that each anion coordinates sufficiently to the(1,5-COD)-Ir^+ moiety to slow down the reduction of Ir(I) to Ir(0) atoms; this, in turn, prevents the otherwise rapid aggregation of Ir(0) atoms to produce bulk metal. However, the finding that even OH^- can avoid bulk metal precipitation, apparently by slowing down nanocluster nucleation and growth, is a point worth noting.

Control Experiment Demonstrating That Classical Types of Polyoxoanions Lacking Surface Oxygen Basicity Do Not Yield Stabilized Nanocluster but Instead Lead to Bulk Ir(0) Metal. Even early on in these studies, control reactions indicated that the intimate involvement of the basic $P_2W_{15}Nb_3O_{62}^{9-}$ polyoxoanion (or, analogously, the basic $SiW_9Nb_3O_{40}^{7-}$ polyoxoanion) with $(1,5\text{-COD})Ir^+$ is a key to avoid the formation of Ir(0) metal particles during the cyclohexene hydrogenation reaction. Specifically, the much more common, commercially available but *nonbasic* polyoxoanions $P_2W_{18}O_{62}^{6-}$ and $SiW_{12}O_{40}^{4-}$ (which are roughly as nonbasic[45] as ClO_4^-), *do not* prevent the formation of Ir(0) metal particles (see the Experimental Section). An explanation for the formation of Ir(0) metal particles is apparent from rewriting $P_2W_{18}O_{62}^{6-}$ as it exists structurally, $\{(PO_4)_2^{6-}(W_{18}O_{54})^0\}$: the very limited, near-zero surface charge of $P_2W_{18}O_{62}^{6-}$ prevents it from binding to $(1,5\text{-COD})Ir(acetone)_2^+$, and the latter is then rapidly reduced to Ir(0) atoms which then aggregate to bulk Ir crystallites. It follows, therefore, that the inhibition of bulk Ir(0) metal formation in the case of $(Bu_4N)_5Na_3[(1,5\text{-COD})Ir\cdot P_2W_{15}Nb_3O_{62}]$ is the result of the three extra units of anionic surface oxygen charge density in $P_2W_{15}Nb_3O_{62}^{9-}$ and thus its relatively strong binding to $Ir(1,5\text{-}COD)^+$.

Evidence for Nucleation by $Ir(0)_{n\rightarrow m}$ Nanocluster Formation through Low-Level $Ir(1,5\text{-COD})(solvent)^+$ Dissociation from $[(1,5\text{-COD})Ir\cdot P_2W_{15}Nb_3O_{62}]^{8-}$ Followed by Its Reduction by H_2 to Ir(0) Atoms during the Observed Induction Period. Although the demonstration of Ir nanocluster formation from the precursor $[(1,5\text{-COD})Ir\cdot P_2W_{15}Nb_3O_{62}]^{8-}$ plus H_2 makes it clear that nucleation to a narrow range of $Ir(0)_{n\rightarrow m}$ nanoclusters must be involved,[2b,5f] the details of this step, and thus the intimate nature of the processes occurring during the induction period, were probed via additional experiments. Based on the high sensitivity of the induction period to H_2O, H^+, and more coordinating solvents as detailed elsewhere[24] (all of which significantly shorten the induction period), and given the literature's indication that low-level Ir(0) formation was likely a key to the narrow size range of nanoclusters found,[2b,5a-c] we hypothesized that solvent- (or H_2O- or H^+-) induced, low-level dissociation of $[(1,5\text{-COD})Ir\cdot P_2W_{15}Nb_3O_{62}]^{8-}$ to $Ir(1,5\text{-COD})(solvent)^+$ and $P_2W_{15}Nb_3O_{62}^{9-}$ was a key first step. This is then followed by rapid reduction of $Ir(1,5\text{-COD})(solvent)^+$ to Ir(0) by H_2 (which was independently demonstrated in a control experiment); these two key steps provide a low-level, reproducible (as long as the H_2O and H^+ are constant), and *continuous* source of Ir(0) that then nucleate to a narrow range of $Ir(0)_{n\rightarrow m}$ nanoclusters.

Consistent with and fully supportive of this suggested mechanism, as little as 7 equiv of $(Bu_4N)_9P_2W_{15}Nb_3O_{62}$ polyoxoanion *completely suppresses* the cyclohexene hydrogenation reaction. Also, the addition of a small amount (0.04 equiv) of $Ir[1,5\text{-COD}](acetone)_2^+$ shortens the induction period by 40% (Figure M, supplementary material). The fact that H^+ also dramatically shortens the induction period, almost surely by releasing $Ir[1,5\text{-COD}](acetone)_2^+$ via the reaction $H^+ + (1,5\text{-COD})Ir\cdot P_2W_{15}Nb_3O_{62}^{8-}$ to give $H_xP_2W_{15}Nb_3O_{62}^{x-9}$ and $Ir(1,5\text{-COD})(solvent)^+$, is yet another piece of evidence for the initial dissociation step and then the subsequent reduction of $Ir[1,5\text{-COD}](acetone)_2^+$ by H_2 to Ir(0) atoms.

Minimum Mechanism for Ir Nanocluster Formation: Homogeneous Nucleation Followed by Autocatalytic Growth. The cyclohexene hydrogenation catalyzed by each Ir precursor studied herein, monitored by a sensitive ±0.01 psig of H_2 pressure transducer to yield curves such as those shown in Figure 9, proceeds

(45) Barcza, L.; Pope, M. T. *J. Phys. Chem.* **1973**, *77*, 1795.

Scheme 2. Minimum Mechanistic Scheme Summarizing (A) the Nucleation and Autocatalytic Formation of Ir(0) Atoms from (1,5-COD)Ir·$P_2W_{15}Nb_3O_{62}^{8-}$ and (B) the Concomitant Reduction of Alkene and Polyoxoanion

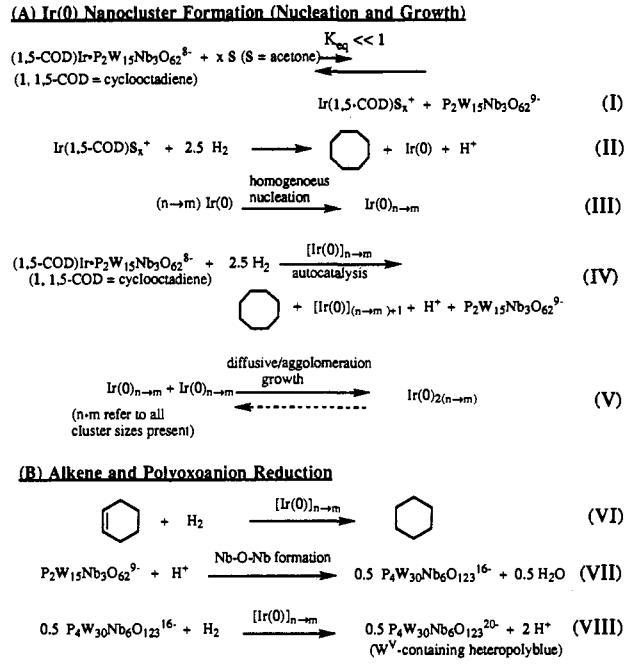

with a pronounced 2.0 ± 0.2 h induction period. The hydrogenation curves, plus the quantitative curve fitting provided elsewhere,[23c,24] demonstrate that the curves seen (e.g., in Figure 9) can be accounted for *only* [23c,24] by an *autocatalytic growth* of the catalytically active Ir nanoclusters. Scheme 2 summarizes a minimum mechanistic scheme (i.e., a scheme that has the minimum number of steps supported by, and necessary to explain, the data herein). Basically, it expands the established stoichiometry and other facts previously summarized in Scheme 1 by adding autocatalytic growth and (diffusive) cluster agglomeration growth steps to complete the proposed minimum mechanism, Scheme 2.

First, there is a dissociation of Ir(1,5-COD)S_x^+ (S = solvent) from (1,5-COD)Ir·$P_2W_{15}Nb_3O_{62}^{8-}$ (**1**) by solvent displacement (step I); the solvated Ir(1,5-COD)S_x^+ is then readily reduced by H_2 to give an Ir(0) atom (step II, Scheme 2). (Note that the 5-coordinate Ir(I) in (1,5-COD)Ir·$P_2W_{15}Nb_3O_{62}^{8-}$ (**1**) is 18 electron and thus unable to activate H_2.)

Second, there is nucleation via diffusive aggregation of Ir(0) atoms into a distribution of $Ir(0)_n$ nanoclusters (step III, Scheme 2). These nucleation steps (I–III) nicely account for the observed induction period and its ±10% reproducibility (10% reproducibility so long as the same batch of acetone solvent, containing the same amount of H_2O and of the same purity, is used). These nucleation steps are necessarily predominantly "homogeneous" [11b] (i.e., depend on the concentration of Ir(0) atoms only) and not "heterogeneous" [46] (i.e., do not depend on impurities in the solution or on the glassware surface). Note that these nucleation and growth steps would seem to be much smoother and *more continuous* (and thus more reproducible) than the popular and often cited (but recently criticized[2b]) "burst" nucleation phenomenon from a supersaturated solution associated with LaMer's mechanism.[5a]

Third, we have quantitative and unequivocal evidence for autocatalytic growth from $Ir(0)_n$ catalysis of hydrogenation of additional (1,5-COD)Ir·$P_2W_{15}Nb_3O_{62}^{8-}$ (**1**) to Ir(0) (hydrogenation of **1** on the nanocluster's surface) (step IV). One crucial feature of such autocatalytic growth is that, once the initial crop of Ir(0) nuclei are formed (with difficulty, in general[47]), few additional Ir nuclei form in comparison to the (autocatalytic) rate of cluster growth—that is, *the separation in time, of nucleation and of cluster growth, is accomplished by the autocatalysis.* It has been pointed out previously that the separation in time, of the nucleation from the growth stages of nanocluster formation, is "the first requirement" for the formation of uniform particles.[48a] Note also that one would expect an autocatalytic path to produce roughly spherical nanoclusters just as we observe (spherical, because diffusion leads to an equal probability of adding an Ir(0) atom to all parts of an existing *spherical* nanocluster's surface, and assuming that the relative rates of the different surfaces of the nanocluster are not drastically different, at least not for a simple hydrogenation reaction). [The shear forces of our stirred solutions are another factor that could favor "Ostwald ripening" leading to spherical particles,[5c,48b] for example, processes such as $Ir(0)_{n\to m}$ to give $Ir(0)_{n\to m-1}$ + Ir(0), or $Ir(0)_{n\to m}$ + Ir(0) to give $Ir(0)_{n\to m+1}$]. Lastly, and despite its current state of underappreciation, there is every reason to expect that autocatalysis of nanocluster growth from the reduction of metal salts with H_2 is a more general phenomenon, especially when starting with coordinatively saturated 18-electron complexes (i.e., where the autocatalytic mode of H_2 activation is necessarily faster than that by the 18-electron organometallic complex), *an insight which contains a key ingredient for the design of other (autocatalytic) nanocluster syntheses.*

Step V, the proposed (presumably reversible) diffusive cluster agglomeration and growth reaction,[5e,49] and a step that logically must exist (i.e., with some finite rate), is the only step in the minimum mechanism in Scheme 2 that is on less solid grounds. However, one additional piece of evidence is fully consistent with a prediction made by the kinetic competition between steps IV and V in Scheme 2. Specifically, noticeably more irregular particles are formed if the nanoclusters are produced at 1 atm of H_2 rather than the normal 2.7 atm (40 psig) (Figure 13). This is fully consistent with the H_2 pressure dependence upon cluster growth *predicted by Scheme 2*; specifically, it suggests that, under our normal conditions of 40 psig of H_2, most of our cluster growth occurs by the autocatalysis pathway[50] (step IV). But, under the lower 1 atm of H_2 pressure conditions, a greater contribution to cluster growth by the agglomeration pathway (step V) can occur, leading to *less spherical particles* [i.e., this is true at least when the agglomeration of two more massive $Ir(0)_{n\to m}$ particles and their morphology are under kinetically controlled, nonsintering conditions (and if stirring shear forces are not operative), so that the agglomerated particles' *initial* composition and morphology are largely retained].

The remaining steps in Scheme 2 are just those that are known from the reaction's established stoichiometry: cyclohexene reduction (step VI) (evidence that the Ir(0) nanoclusters are indeed the true catalyst is presented in another paper[24]); H^+

(46) Xue, Z.; Thridandam, H.; Kaesz, H. D.; Hicks, R. F. *Chem. Mater.* **1992**, *4*, 162.

(47) (a) The heat of vaporization of Ir metal is 159 kcal/mol, showing the high thermodynamic instability that accompanies (unsolvated) Ir(0) formation: Porterfield, W. W. *Inorganic Chemistry*; Addison-Wesley Publishing: Reading, MA, 1983; p 84. (b) The formation of a new phase (e.g., Ir nuclei in our case) is furthermore difficult due to the extra surface energy of small clusters: Adamson, A. W. *Physical Chemistry of Surfaces*; A Wiley-Interscience Publication: New York, 1990; p 364.

(48) (a) Sugimoto, T. *Adv. Colloid Interfacial Sci.*, **1987**, *28*, 65–108 (see p 67). (b) Sugimoto, T. *J. Colloid Interface Sci.* **1992**, *150*, 208.

(49) Weitz, D. A.; Lin, M. Y.; Lindsay, H. M.; Haung, J. *Phys. Rev. Lett.* **1987**, *58*, 1052.

(50) Whitesides and co-workers have provided detailed studies of the Pt(0)-surface catalyzed growth of Pt(0) particles from Pt(1,5-COD)R_2 (R = alkyl), work which provides the best available precedent for the Ir cluster growth step in Scheme 2 (although compelling evidence for its autocatalytic nature was not previously available). (a) McCarthy, T. J.; Shih, Y.-S.; Whitesides, G. M. *Proc. Natl. Acad. Sci. U.S.A.* **1981**, *78*, 4649. (b) Whitesides, G. M.; Hackett, M.; Brainard, R. L.; LaVelleye, J. P.-P.; Sowinski, A. F.; Izumi, A. N.; Moore, S. S.; Brown, D. W.; Staudt, E. M. *Organometallics* **1985**, *4*, 1819. (c) Miller, T. M.; Izumi, A. N.; Shih, Y.-S.; Whitesides, G. M. *J. Am. Chem. Soc.* **1988**, *110*, 3146. (d) Lee, T. R.; Whitesides, G. M. *Acc. Chem. Res.* **1992**, *25*, 266, and references therein to the other papers in this series.

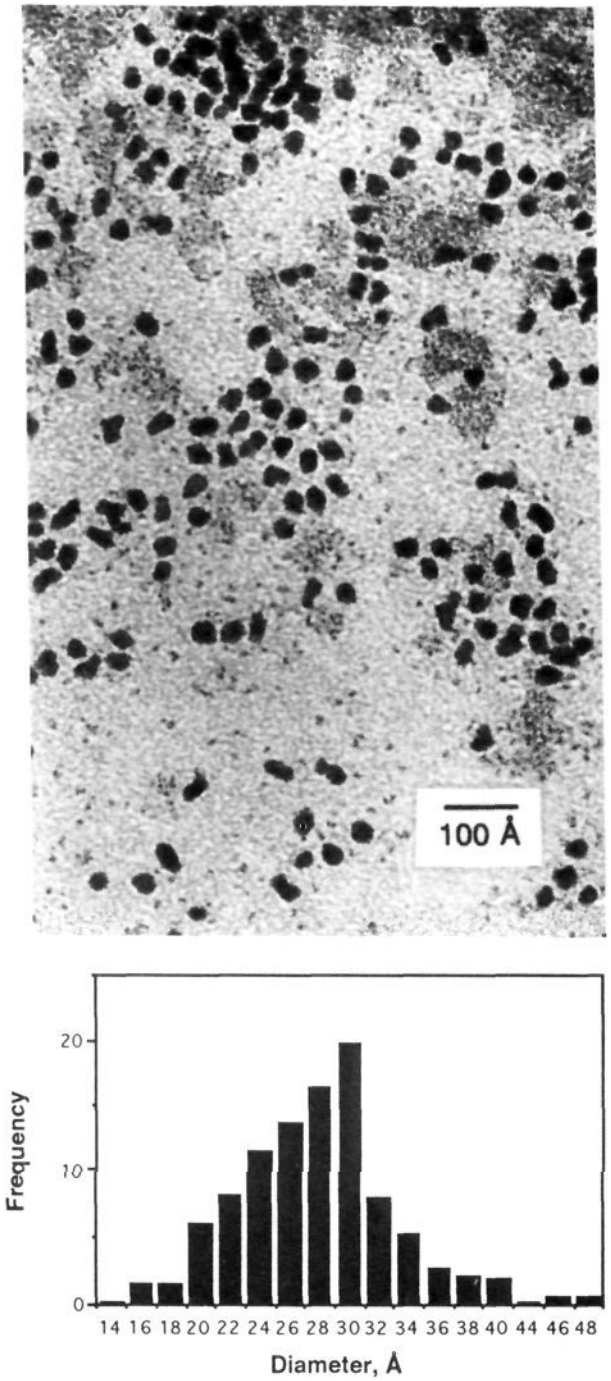

Figure 13. (A) (top) TEM of the Ir nanoclusters prepared from reduction of $(Bu_4N)_5Na_3[(1,5\text{-COD})Ir{\cdot}P_2W_{15}Nb_3O_{62}]$ *under the lower pressure of 1 atm (14.7 psig) of H_2 atmosphere.* (B) (bottom) Histogram of the Ir nanocluster sizes (estimated diameters). The mean diameter is 27.8 Å, with a standard deviation of 3.7 Å, from a sample population of 508. Note that these nanoclusters are less spherical, and more irregular, than the nanoclusters prepared at 2.7 atm (40 psig) of H_2.

induced formation of the Nb–O–Nb aggregate to the observed product, $P_4W_{30}Nb_6O_{123}^{16-}$,[31] and then its independently verified and quantitated four-electron reduction to the four W^V-containing "heteropolyblue",[27] $P_4W^{VI}{}_{26}W^V{}_4Nb_6O_{123}^{20-}$.

Several points are especially noteworthy from the mechanism proposed in Scheme 2, specifically the evidence for (i) a *continuous* nucleation pathway involving a probably quite low [Ir(0)] (a finding that would seem to challenge the old, widely quoted burst type of nucleation process for the formation of a narrow distribution of nanoclusters[46]) and (ii) competing growth pathways consisting of autocatalytic growth involving an Ir nanocluster surface reaction,[50b] in competition with diffusive agglomeration of $Ir(0)_{n\rightarrow m}$ particles. (Diffusion vs reaction-chemistry-controlled colloid growth steps are the topic of a recent *Nature* paper providing evidence that these steps are universal in colloid aggregation.[5d]) The resultant, near monodispersity (i.e., within ±15%) of the polyoxoanion-stabilized Ir nanocluster formed in these studies goes far toward explaining why the structure-insensitive reaction[23d] studied herein (cyclohexene hydrogenation) exhibits a 10% kinetic reproducibility, a little precedented and initially quite surprising finding.[24] Additional noteworthy points about the present system are (iii) it has allowed one of the more detailed mechanistic investigations to date on the formation of a narrow dispersion of *transition metal* nanoclusters; (iv) this study comes at a time when a call for additional mechanistic understanding has been made;[2b] and (v) the mechanism proposed in Scheme 2 suggests a number of other experiments to test and refine this mechanism (which is by no means considered complete; additional experiments are planned to test quantitatively key variables such as the H_2 pressure, the solvent viscosity, the reactant concentrations, the temperature, and so on).

Summary

The highlights of the present work can be summarized as follows:

(1) $Ir_{\sim 300}$ and $Ir_{\sim 900}$ polyoxoanion/Bu_4N^+-stabilized, organic solvent-soluble nanoclusters that are new compositions of matter, that can be reproducibly prepared, and that are of a narrow, ±15%, size distribution have been prepared in the absence of oxygen from the reduction of $(Bu_4N)_5Na_3[(1,5\text{-COD})Ir{\cdot}P_2W_{15}Nb_3O_{62}]$ under H_2, with ($Ir_{\sim 300}$) and without ($Ir_{\sim 900}$) cyclohexene present. The polyoxoanion component of these nanoclusters is without prior precedent, and the present invention requires the use of custom-made, *basic* polyoxoanions such as $P_2W_{15}Nb_3O_{62}^{9-}$ and $SiW_9Nb_3O_{40}^{7-}$ (control experiments with nonbasic, classical types of nonbasic polyoxoanions, and which do not yield polyoxoanion-stabilized nanoclusters, prove this point). The average chemical composition of the isolated $Ir_{\sim 900}$ nanoclusters is $[Ir(0)_{\sim 900}(P_4W_{30}Nb_6O_{123}^{16-})_{\sim 60}](Bu_4N)_{\sim 660}Na_{\sim 300}$, while that of the smaller $Ir_{\sim 300}$ nanoclusters is $[Ir(0)_{\sim 300}(P_4W_{30}Nb_6O_{123})_{\sim 33}](Bu_4N)_{\sim 300}Na_{\sim 233}$ (where the polyoxoanion is present in the isolated sample in its oxidized, non-heteropolyblue, $P_4W_{30}Nb_6O_{123}^{16-}$ form).

(2) The new $Ir_{\sim 300\text{-}900}$·polyoxoanion nanoclusters have been characterized by TEM, electron diffraction, electrophoresis, ultracentrifugation MW analyses, fast-atom bombardmemt mass spectroscopy, elemental analysis, IR and UV–visible spectroscopy, and a number of appropriate control experiments.

(3) The $Ir_{\sim 300\text{-}900}$·polyoxoanion nanoclusters are unusual in that they are stabilized enough so that they may be *isolated* and later redissolved in organic solvents without detectable changes in their size or aggregation by TEM. Electrophoresis and ion-exchange resin studies indicate an overall negative charge on the nanocluster in solution and, therefore, that the $P_2W_{15}Nb_3O_{62}^{9-}$ polyoxoanion must be adsorbed onto the neutral Ir(0) nanocluster surface, a conclusion reinforced by two other lines (four total) of evidence. Elemental analysis confirms that the 9:1 and 15:1 Ir:polyoxoanion ratios for the $Ir_{\sim 300}$ and $Ir_{\sim 900}$ nanoclusters, respectively, mirror those calculated assuming a simple geometrical model for adsorption of close-packed $P_2W_{15}Nb_3O_{62}^{9-}$ onto the nanocluster's surface. TEM further confirms that, if some of the nanocluster-stabilizing $(Bu_4N)_9P_2W_{15}Nb_3O_{62}$ is deliberately removed by precipitating the nanoclusters with ether, then extensive agglomeration of the nanoclusters occurs.

(4) The narrow size distribution, plus probably that a structure-insensitive reaction, cyclohexene hydrogenation, was chosen for initial study, leads to a high level of reproducibility in the catalytic

activity (±10%), a degree of reproducibility virtually undocumented previously in metal colloid or nanocluster catalysis, and a degree of reproducibility traditionally associated with single-metal homogeneous catalysts. In addition, it is significant that the *nanoclusters exhibit absolute rates of catalytic activity that are as high as any homogeneous or oxide-supported heterogeneous Ir(0)$_x$ sample tested.*[24]

(5) The stabilization of the polyoxoanion is of a little precedented type,[51] one *apparently* due to the *combined high charge* plus *significant steric bulk present intrinsically* within both the *poly*anion and *poly*-Bu_4N^+ cation components of $(Bu_4N^+)_9(P_2W_{15}Nb_3O_{62}^{9-})$. Further studies of other polyanions with other R_4N^+ countercations will be needed, and are planned, to better understand this unusual stabilization mode.

(6) The somewhat oxidizing polyoxoanion captures reducing ($H^\bullet$) equivalents from the Ir nanoclusters ("$H^\bullet$ spillover"), thereby producing a heteropolyblue and effectively cleaning the nanocluster's surface of reducing equivalents. Further studies will be required here as well (e.g., of non-polyoxoanion polyanions) in order to fully understand the catalytic effects, and other conceivable applications, of this little precedented aspect of having a *chemically reactive and tunable redox component* (the polyoxoanion) as part of the nanoclusters.

(7) Considerable evidence on the mechanism of nanocluster formation was provided, specifically evidence (a) for a smooth, low [Ir(0)] nucleation mechanism (produced by H_2 reduction of $Ir(1,5\text{-COD})(acetone)_2^+$ that has first dissociated from the $(Bu_4N)_5Na_3[(1,5\text{-COD})Ir{\cdot}P_2W_{15}Nb_3O_{62}]$ precursor) and (b) for autocatalytic growth on the developing Ir nanocluster's surface (plus, under lower H_2 levels, preliminary evidence interpreted in terms of competing $Ir(0)_{n\rightarrow m}$ nanocluster diffusive agglomeration). The little recognized autocatalytic growth step is key in that it accomplishes the *separation in time* of the nucleation and growth stages of nanocluster formation, an essential step for monodispersed nanocluster syntheses (i.e., where growth is not physically constrained, for example, by the use of micelles).

(8) The autocatalytic growth mechanism is predicted to be common for nanocluster reductive formation reactions of 18-electron precursor complexes with H_2; it and its modifications offer, therefore, a new design feature which can be built into syntheses aimed at the central problem of the production of monodispersed nanoclusters. The present system is also one that should allow additional mechanistic studies, ones focused toward developing other general principles for the formation of monodispersed transition metal particles.

(9) Since polyoxoanions can be regarded as discrete fragments of solid oxides,[52] the soluble polyoxoanion "oxide-supported" Ir nanoclusters can be regarded as the first discrete analogs of the commercially important solid-oxide-supported small Ir particles in heterogeneous catalysts. Consistent with and supportive of this view is the observation of H_2 spillover leading to reduced heteropolyblue complexes, results which provide the first discrete, soluble analog of H_2 spillover.

(10) The high reactivity of the Ir·polyoxoanion nanoclusters, a reactivity indistinguishable from solid-oxide-supported Ir(0),[24] plus their solubility in homogeneous solution (thereby making NMR, kinetic, and other powerful solution methods available to their study) make polyoxoanion-stabilized metal(0) nanoclusters of considerable interest for detailed mechanistic studies, especially of the fundamental concepts and underlying classes of reactions and their mechanisms in heterogeneous catalysis. The intrinsic reactions and reactivity of polyoxoanion-stabilized metal(0) nanoclusters should prove of interest as well, and both of these areas are high priorities of efforts in progress.

(11) Finally, the discovery of isolable and redissovable ±10% reproducible reactivity Ir(0) nanoclusters, when beginning with a homogeneous $Ir^I(1,5\text{-COD})^+$ complex, $[(1,5\text{-COD})Ir{\cdot}P_2W_{15}Nb_3O_{62}]^{8-}$, teaches that the formation of hybrid homogeneous–heterogeneous nanocluster catalysts in a reductive catalytic reaction (and when starting with a discrete metal complex precatalyst) is a mechanism that must be given very serious consideration when attempting to discern the true catalyst in an otherwise "homogeneous" catalyst.

In another paper,[24] we present a more general approach and solution to the so-called "homogeneous vs heterogeneous" mechanistic problem, an approach which led to the discovery of the new, hybrid homogeneous–heterogeneous[24] Ir·polyoxoanion nanoclusters reported herein.

Experimental Section

Materials. $[(1,5\text{-COD})IrCl]_2$, $(Bu_4N)_5Na_3[(COD)Ir{\cdot}P_2W_{15}Nb_3O_{62}]$,[25] and $(Bu_4N)_4Na_2[(1,5\text{-COD})Ir{\cdot}SiW_9Nb_3O_{40}]$[42] were prepared according to the literature cited; their purity was checked by ^1H or ^{31}P NMR spectroscopy. All commercially obtained compounds were used as received unless indicated otherwise: acetone (Burdick and Jackson, 0.22% H_2O), Bu_4NOH (40% in water, Aldrich, freshly opened), $(NH_4)_2Ce(NO_3)_6$ (Aldrich), $AgBF_4$ (Aldrich, purified by extraction with diethyl ether and followed by evaporation of the extract under vacuum to give a white powder), cyclohexane (Baker), acetonitrile (Baker, distilled from CaH_2 under N_2), cyclohexene (Baker, run through a Brockman activity (I) basic alumina column and then distilled from Na under N_2). Hydrogen gas (Air Products, 99%) was purified by its passage through an indicating moisture trap, a O_2 cartridge, and an indicating O_2 trap (Scott). Unless noted otherwise, all experiments were performed in a Vacuum Atmospheres drybox (<1 ppm of O_2 by a Vacuum Atmospheres O_2 analyzer gauge).

Instrumentation and Analytical Procedures. Air-sensitive materials were routinely handled in a Vacuum atmospheres inert atmosphere drybox. Visible spectra were recorded on a Beckman DU-7 spectrophotometer using 1-cm cuvettes equipped with Teflon stoppers for air-sensitive samples. IR spectra were measured as KBr pellets using a Nicolet 5DX spectrometer. FAB-MS were recorded on a Kratos MS-50 mass spectrophotometer at Oregon State University by Dr. Brian Arbogast, using a matrix of 5:1 dithiothreitol:dithioerythritol. Xenon gas was used to generate the primary ionizing beam from an Ion-Tech FAB gun operated at 7–8 keV. Gas–liquid chromatography was performed on a Hewlett-Packard HP5970A GC equipped with a HP 3390A integrator and a Alltech Econo-cap capillary carbowax column (30 m × 0.25 mm). The column temperature was controlled by the following temperature program in the GC studies: initial temperature of 35 °C for 4.0 min, ramped at 15 °C/min to a final temperature of 200 °C, and held there for 1.0 min, followed by cooling back to 35 °C.

Transmission Electron Microscopy and Electron Diffraction Studies. Transmission electron micrographs were taken on a Philips CM-12 with a 70-μm lens operated at 100 kV and with a point-to-point resolution of 2.0 Å (measured using single-crystal gold). Electron diffraction patterns were taken on the same instrument with a 530-mm camera length with the selected area containing hundreds of Ir particles. Samples for both TEM and electron diffraction studies were prepared by spraying the Ir nanocluster solution onto a copper grid covered with an amorphous carbon thin film. Control experiments showed that the same TEM image was obtained whether the sample was sprayed in N_2 or air. An alternative TEM sample preparation method, involving the placement of a small drop of the nanocluster solution onto a grid followed by removal of any extra solution and drying in air for 1 min, gave the same TEM image. Additional control experiments showed that changing the voltage (40 vs 100 kV) or the exposure time (seconds vs minutes) did not change the TEM images or electron diffraction patterns; hence, all samples examined appear to be beam-stable. In addition, all samples were examined at both low (100 K) and high (430 K) magnification from at least three randomly chosen areas. Furthermore, at least two samples from two independent runs (at the same reaction conditions) were examined. Thus

(51) (a) Stabilization of colloids by lower charged polyanions, notably citrate[5,51b,c] or $(NaPO_3)_6$,[5f] is known, however, as is the use of the ill-defined[51d] mixture of complexes known as "polyphosphate", $[-(P_nO_{3n+1})-]^{-n-2}$.[51e] (b) Turkevich, J. *J. Chem. Phys.* **1945**, *13*, 235. Turkevich, J.; Stevenson, P. C.; Hillier, J. *Discuss. Faraday Soc.* **1951**, *11*, 55. Turkevich, J.; Kim, G. *Science* **1970**, *169*, 873. (c) Brugger, P.-A.; Cuendet, P.; Grätzel, M. *J. Am. Chem. Soc.* **1981**, *103*, 2923. (d) Cotton, F. A.; Wilkinson, G. "Advanced Inorganic Chemistry"; 3rd ed.; Interscience: New York, 1972; p 397–398. (e) Henglein, A. *Chem. Phys. Lett.* **1989**, *154*, 473.

(52) Baker, L. C. W. In *Advances in the Chemistry of Coordination Compounds*; Kirschner, S., Ed.; MacMillan: New York, 1961; p 604.

the TEM and electron diffraction studies appear to be truly representative of the samples and the different runs done at the same conditions.

Solution Molecular-Weight Measurements. Solution molecular weights, MW, determined by the ultracentrifuge sedimentation–equilibrium method,[30] were carried out on a Beckman Instruments Spinco Model E ultracentrifuge equipped with a scanning photoelectric system and an on-line IBM-compatible computer. Samples for MW determinations were prepared in a N_2 atmosphere drybox by dissolving the Ir nanocluster powder sample in 0.1 M Bu_4NPF_6/CH_3CN electrolyte solution, and the concentration of the sample was adjusted so that the absorbance at the desired wavelength falls between 0.3 and 0.6 absorbance units. The sample was then placed into a doubly-sectored cell which is specifically designed for MW measurements. The cell was taken out of the drybox, loaded into a rotor, and then spun at the specified speed. (Note that it is, of course, essential to use the proper rotation speed in order to get the ultracentrifuge sedimentation equilibrium of the species *one hopes to detect*, and that the required rotation speed depends upon the molecular weight of the species in question.) After sedimentation–equilibrium was achieved (as determined by no further change in the concentration–distribution curve over an additional 24 h of ultracentrifugation), the concentration vs distance (r) data were then collected and analyzed by a locally written program on the on-line computer. A plot of ln(absorbance) vs r^2 together with the best linear fit is then obtained. The molecular weight, MW, is then calculated according to the following equation:

$$\text{molecular weight} = \frac{2RT}{(1-\nu\rho)\omega^2}\frac{d\ln C}{dr^2}$$

where $R = 8.314 \times 10^7$ J K^{-1} mol^{-1}, ν is the partial specific volume of the sample, ρ is the density of the electrolyte solution, $\omega = 2\pi/60$ (rpm), and $(d \ln C)/dr^2$ is the slope obtained from a plot of ln A (absorbance) vs r^2 (r is the distance from the center of the rotor). The temperature, measured at the end of each run, was 21 ± 1 °C. The density of the electrolyte solution, 0.78 g/cm^3 in acetonitrile solution, was experimentally determined, while the partial specific volume, a key variable in these MW determinations, was approximated by the apparent specific volume which in turn was measured using a 25-mL pycnometer. Using this method, the apparent specific volumes of $(Bu_4N)_9P_2W_{15}Nb_3O_{62}$ and its aggregates, $(Bu_4N)_{12}H_4P_4W_{30}Nb_6O_{123}$, are all within 0.4 ± 0.06.[31] The apparent specific volume of Ir nanoclusters was approximated from the density of bulk Ir(0) metal (22.5 g/cm^3) to be 0.04 cm^3/g, which should be a close approximation since electron diffraction studies demonstrates that the Ir nanoclusters are cubic close-packed as in bulk Ir metal.

As a control against air leakage into the double-sector cell during data collection on air-sensitive samples, an approximately 1×10^{-6} M solution of the very air-sensitive, deep blue cobalt(I) complex[53] $[Co^I(CO)\{C_2(DO)(DOH)_{pn}\}]$ in 0.1 M $[(n\text{-}C_4H_9)_4N]PF_6/CH_3CN$ was placed into the cell in the drybox. This cell was then placed under the experimental conditions (a hard vacuum an 20 000 rpm for 24 h) and then subsequently placed on the lab bench for 48 h. During this 72 h period (more than three times the length of the typical molecular-weight experiment), no visual loss of the deep blue color was noted, demonstrating that no significant leakage of O_2 into the cell occurred over the course of a typical molecular-weight experiment. The above control experiment was done by D. Lyon.[23b]

(1) Solution Molecular-Weight Measurements on $Ir_{\sim 900}$-Polyoxoanion (Sample I). Two separate experiments were done under different conditions (different rotation speeds and different detection wavelengths) in order to determine, separately, the molecular weights of the Ir nanoclusters and the polyoxoanion present in the sample. Specifically, for the molecular-weight measurement on the $Ir_{\sim 900}$ nanoclusters, the sample was prepared in the drybox by dissolving $Ir_{\sim 900}$-polyoxoanion (sample I) in 0.1 M Bu_4NPF_6/CH_3CN electrolyte solution (ca. 1 mg/mL) and the concentration was further adjusted so that the absorbance in the 420–460-nm range falls between 0.3 and 0.6 absorbance units. The sample was then placed in the double-sector cell, which was then taken out of the drybox and loaded into a rotor. The sample was then spun at 4000 rpm. After 17 h, equilibrium was established (as judged by no further change in the concentration distribution after an additional 24 h). The concentration distribution was analyzed at wavelengths ranging from 420 to 460 nm (a wavelength range appropriate for the Ir nanoclusters; see Figure C, supplementary material); each wavelength gave the same *nonlinear* plot of ln(absorbance) vs r^2 (Figure D, supplementary material), confirming the inhomogeneity of the sample[54] as independently verified by TEM (i.e., a distribution of nanoclusters is present, recall Figure 4). A weight-average molecular weight, $\overline{M}_r$, of $(1.8 \pm 0.8) \times 10^5$ was obtained from the best linear fit of the curve plot and from the assumption that the partial specific volume must lie close to that estimated for bulk Ir metal (i.e., 0.04 cm^3/g, from inverting the density of Ir metal, 22.5 g/cm^3; a measurement of the partial specific volume for the Ir nanoclusters is impossible experimentally, due to interference of the large amount of free polyoxoanions which stabilize the Ir nanoclusters and thus cannot be removed). The error bars were estimated by the slopes from lower and higher portions of the curve. The measured $\overline{M}_r$ of $(1.8 \pm 0.8) \times 10^5$ agrees quite well with the expected MW for the 30-Å ca. $Ir_{\sim 900}$ nanoclusters, $MW(Ir_{900}) = 1.7 \times 10^5$.

For molecular-weight measurement of the polyoxoanions present in the same sample ($Ir_{\sim 900}$-polyoxoanion (sample I)), the same solution used in the molecular-weight determination of the Ir nanoclusters was diluted (ca. 100 times) until the absorbance of the solution at 280 nm was between 0.3–0.6 units. The sample was placed in a double sector cell; the latter was then loaded in a rotor and spun at a rotation speed of 20 000 rpm. Sedimentation–equilibrium was established after 17 h, and the concentration distribution was analyzed at wavelengths ranging from 280 to 350 nm (a wavelength appropriate for polyoxoanions, see Figure C, supplementary material); each wavelength gave the same linear plot of ln(absorbance) vs r^2 (Figure G, supplementary material). MW = 12 000 ± 2000 on the basis of the slope of the plot and a measured[31a] partial specific volume of 0.37 cm^3/g for the polyoxoanion. The measured MW of 12 000 ± 2000 agrees quite well with that calculated, 11 078, for $(Bu_4N)_{12}H_4P_4W_{30}Nb_6O_{123}$.

(2) Solution Molecular-Weight Measurements on $Ir_{\sim 300}$-Polyoxoanion (Sample II). In the exact same manner as described for $Ir_{\sim 900}$-polyoxoanion (sample I), two separate molecular-weight experiments were carried out on $Ir_{\sim 300}$-polyoxoanion (sample II). The average molecular weight ($\overline{M}_r$) of the $Ir_{\sim 300}$ nanoclusters was estimated to be $(8.6 \pm 4.0) \times 10^4$, from the *nonlinear* plot (Figure J, supplementary material) and again with the assumption that the partial specific volume must lie close to 0.04 cm^3/g, an estimate derived from inverting the density of bulk Ir metal (22.5 cm^3/g). The error bars were estimated by the slopes from lower and higher portions of the curve. The measured $\overline{M}_r$ of $(8.6 \pm 4.0) \times 10^4$ is consistent with the MW calculated for Ir_{300} (MW (Ir_{300}) = 57 660). The MW of the polyoxoanion present in the sample was determined to be 10 800 ± 2000, on the basis of the slope of the linear plot (Figure K supplementary material) and a measured[31a] partial specific volume of 0.37 cm^3/g for the polyoxoanion. This measured MW of 10 800 ± 2000 agrees quite well with the calculated MW of 11 078 for $(Bu_4N)_{12}H_4P_4W_{30}Nb_6O_{123}$.

Hydrogen Uptake Stoichiometry Studies. In the drybox, $(Bu_4N)_5Na_3[(1,5\text{-COD})Ir\cdot P_2W_{15}Nb_3O_{62}]$ (150 mg, 2.26×10^{-2} mmol, 8.81 mM) was dissolved in 2.0 mL of acetone-d_6 (slightly less than a saturated solution). The solution was then pipetted into a 97 cm^3 of H_2 uptake flask equipped with a Teflon stopcock. The flask was sealed under N_2, removed from the drybox, and attached to a vacuum line. The total volume of the vacuum system employed was either 87 ± 3 cm^3 (a small pressure tube) or 200 ± 5 cm^3 (a converted, 100 mL round-bottom flask) as measured by the pressure change following the opening of a stopcock to a standard calibrated flask (54.9 cm^3, at 1 atm). The solution was degassed by cycling through four freeze–pump–thaw cycles. The solution was then warmed to −77 °C (dry ice–acetone bath) and 250 mmHg of H_2 was introduced into the flask. The H_2 gas purity was confirmed by GC using a molecular sieve column (13×, isothermal column temperature of 25 °C, He or N_2 carrier gas, thermal conductivity detector). The temperature was then raised to 22.0 ± 0.1 °C. Over 32 h, 3.5 ± 0.3 equiv of H_2 was consumed (Figure 7), giving a deep brown precipitate and a blue solution (due to heteropolyblue[29] formation), which changed to amber over 5 min after the H_2 atmosphere was released. The uptake of gas (the pressure decrease) was directly measured by a manometer. Control experiments showed negligible uptake of H_2 in the absence of added compound. The uptake solution was analyzed by ^{1}H NMR and GC spectroscopy to contain 1 equiv of cyclooctane. (The above experiment was done by D. Lyon, pages 61 and 90 of ref 23b).

Preparation of 30 ± 4 Å $Ir_{\sim 900}$ Nanoclusters (Sample I) from the Reaction of $(Bu_4N)_5Na_3[(1,5\text{-COD})Ir\cdot P_2W_{15}Nb_3O_{62}]$ with H_2. In the drybox, 1.0 g of $(Bu_4N)_5Na_3[(1,5\text{-COD})Ir\cdot P_2W_{15}Nb_3O_{62}]$ (0.176 mmol)

(53) Finke, R. G.; Smith, B. L.; McKenna, W. A.; Christian, P. A. *Inorg. Chem.* **1981**, *20*, 687.

(54) Hiemenz, P. C. *Principles of Colloid and Surface Chemistry*; Marcel Dekker: New York, 1977; p 120–121.

was dissolved in 150 mL of acetone to give a clear-yellow solution (1.2 mM). The solution was then transferred into a 460-mL Fisher–Porter bottle which had been equipped with Swagelok TFE-sealed quick-connect. Next, the bottle was removed from the drybox and connected to a H_2 line and 40 psig of purified H_2 was introduced. (A more detailed description of the apparatus is available elsewhere.[24]) The reaction was initiated by stirring the solution vigorously and then stopped 8 h later when the reaction solution was deep-blue. (The development of the deep-blue color is due to the formation of a well-known W^V-containing heteropolyblue[27] as discussed in the text.) The deep-blue solution was brought into the drybox and filtered through No. 2 Whatman paper to remove a small amount (<5%) of black precipitate (presumably bulk Ir(0) metal particles). A blue filtrate was then obtained, which gradually turned amber within approximately 30 min in drybox, due presumably to $Ir_{\sim 900}$ catalysis of H_2 reevolution (i.e., H_2 evolution from the W^V- and H^+-containing heteropolyblue). A control experiment, in which the heteropolyblue was deliberately exposed to air, showed an immediate change of the blue solution to an amber solution. The amber solution was characterized by TEM (Figures A and B, supplementary material) and UV–visible spectroscopy (Figure C, supplementary material). TEM showed that the amber solution contains ca. 30-Å Ir nanoclusters which are mostly well dispersed in the polyoxoanion matrix as discrete particles, although some floccules of Ir nanocluster aggregates are also found.

The procedure described next allows the removal of extra (i.e., free uncoordinated) polyoxoanions and the isolation of the ca. 30-Å nanoclusters/polyoxoanion/Bu_4N^+ sample as a black powder. To the clear-amber solution of the $Ir_{\sim 900}$ nanoclusters, cyclohexane was added dropwise until the solution turned cloudy and a brown precipitate formed. After standing for approximately 1 h, the light-amber (slightly turbid) supernatant containing the polyoxoanions and a small amount of Ir nanoclusters was removed by pipette. The remaining dark-brown precipitate was rotoevaporated to dryness and then redissolved in acetone to give a clear, amber solution, and the Ir nanoclusters were isolated, again, by careful addition of cyclohexane until the solution turned cloudy. After the removal of the colorless supernatant, the remaining dark-brown precipitate was then evacuated overnight at room temperature to yield a black powder (120 mg, 70% based on Ir). This isolation procedure has been successfully repeated three times. In all cases, the resultant black Ir cluster powder is soluble in acetone (and more soluble in acetonitrile) to give a clear, amber solution of ca. 30-Å $Ir_{\sim 900}$ nanoclusters. The $Ir_{\sim 900}$ nanoclusters so prepared are stable in solution for at least 3 months at room temperature in the drybox, as judged by lack of bulk Ir(0) precipitate. However, upon heating of the clear-amber acetone solution of the nanoclusters at 50 °C for two days, the solution turned faint-amber and a dark precipitate was observed, indicating that aggregation of the Ir nanoclusters had occurred at this higher temperature.

The $Ir_{\sim 900}$ nanoclusters were characterized by TEM (Figure 5) and electron diffraction (Figure 6). Further characterization was accomplished by elemental analysis, IR, FABMS, and solution molecular-weight measurements. Anal. of the $Ir_{\sim 900}$ nanoclusters (sample I) (Pascher, Germany, under N_2). Found: C, 14.48; H, 2.67; N, 1.02; P, 0.84; Ir, 20.1; O, 14.5. Calcd for $[Ir_{15}(P_4W_{30}Nb_6O_{123})(Bu_4N)_{11}Na_5]_{\sim 60}$: C, 15.28; H, 2.89; N, 1.11; P, 0.89; Ir, 20.8; O, 14.23. IR (KBr pellet, cm^{-1}): 1088, 947, 920, 896, and 774 (Figure E, supplementary material); these bands are characteristic of $P_2W_{15}Nb_3O_{62}^{9-}$ polyoxoanion or its Nb–O–Nb bridged aggregate, $P_4W_{30}Nb_6O_{123}^{14-}$.[31] The positive ion FAB-MS (5:1 dithiothreitol:dithioerythritol matrix (Figure F, supplementary material)) exhibited two broad peaks centered around 5000 and 10 000, corresponding to that of $[(Bu_4N)_{10-x-y}Na_xH_yP_2W_{15}Nb_3O_{60}]^+$ and its aggregate $[(Bu_4N)_{17-x-y}Na_xH_yP_4W_{30}Nb_6O_{123}]^+$, respectively. The weight-average MW of the Ir nanoclusters, $\bar{M}_r$, was $(1.8 \pm 0.8) \times 10^5$ (Figure D, supplementary material). The measured MW of the polyoxoanion included in the same sample was 12 000 ± 2000 (Figure G, supplementary material); the calculated MW of $P_4W_{30}Nb_6O_{123}^{16-}$ is 10 593. Electrophoresis and reactions of the Ir nanoclusters with ion-exchange resins are described next. (Details for the molecular-weight measurements were given earlier in the Experimental, Solution Molecular-Weight Measurements Section.)

Experiments Demonstrating That the Nb–O–Nb Bridged Polyoxoanion Aggregate $(Bu_4N)_{12}H_4P_4W_{30}Nb_6O_{123}$ Is Reducible by H_2 To Give a Heteropolyblue. In the drybox, 19.6 mg (1.77×10^{-3} mmol, 0.59 mM) of $(Bu_4N)_{12}H_4P_4W_{30}Nb_6O_{123}$ was dissolved in 3.0 mL of Burdick and Jackson acetone. To the clear, colorless solution was added 28.8 mg of gray powder of 1% Ir/Al_2O_3 (1.50×10^{-3} mmol, 7.9% dispersed). The slurry was then transferred into an 18- × 150-mm disposable borosilicate culture tube which contained a 0.5-in. stir bar. The tube was placed in a Fischer–Porter bottle, which had been modified with Swagelok TFE-sealed quick-connects, and was then sealed. The Fischer–Porter bottle was removed from the drybox, attached to a H_2 line, and purged 15 times with 40 psig of H_2. The reaction was then initiated by stirring the solution vigorously. After 1 h, the solution turned blue. The reaction was stopped, and the Fischer–Porter bottle was brought into the drybox. After being filtered through Whatman No. 2 paper in the drybox (≤1 ppm of O_2), the blue solution turned colorless immediately.

Quantitative Determination of the Heteropolyblue Generated from $(Bu_4N)_5Na_3[(1,5\text{-COD})Ir\cdot P_2W_{15}Nb_3O_{62}]$ by Hydrogen Reduction at 22 °C. (1) Generation of the Heteropolyblue under 400 mmHg of H_2. In the drybox, 126.0 mg (0.0222 mmol, 1.2 mM) of $(Bu_4N)_5Na_3[(1,5\text{-COD})Ir\cdot P_2W_{15}Nb_3O_{62}]$ was dissolved in 18 mL of Burdick and Jackson acetone to give a clear-yellow solution. The solution was then transferred into the Fischer–Porter bottle containing a 0.5-in. stir bar. The Fischer–Porter bottle was brought out of the drybox and attached to the H_2 line via the quick-connects, and 40 psig of H_2 was introduced by purging with 40 psig of H_2 15 times. Then the reduced pressure of 400 mmHg was obtained by expanding the hydrogen gas (70 mL) in the Fischer–Porter bottle to a previously evacuated round-bottom flask (430 mL). The reaction was initiated by vigorous stirring. The reaction was stopped 45 h later; an intense blue solution was obtained.

(2) Generation of the Heteropolyblue under 40 psig of H_2. In the drybox, 120.3 mg (0.0212 mmol, 1.2 mM) of $(Bu_4N)_5Na_3[(1,5\text{-COD})Ir\cdot P_2W_{15}Nb_3O_{62}]$ was dissolved in 18 mL of Burdick and Jackson acetone to give a clear-yellow solution. The solution was then transferred into the Fischer–Porter bottle containing a stir bar. The Fischer–Porter bottle was brought out of the drybox and attached to the H_2 line via the quick-connects, and 40 psig of H_2 was introduced by purging with 40 psig of H_2 for 15 times. The reaction was then initiated by vigorous stirring. An intense blue color was first observed ca. 4 h later, and the reaction was stopped 26 h later.

(3) Titration of the Heteropolyblue Samples. A light-yellow solution of 5.07 mM titrant, $(NH_4)_2Ce(NO_3)_6$, was prepared by dissolving 27.8 mg (0.0507 mmol) in 10.0 mL of 0.1 N H_2SO_4. (The use of 0.1 N H_2SO_4 is necessary to stabilize the Ce(IV) solution.[55]) The solution was degassed by three cycles of freeze–pump–thaw and then brought into the drybox. Meanwhile, in the drybox, 1.0 mL of the heteropolyblue generated at 400 mmHg was taken from the gas-purge outlet of the Fischer–Porter bottle (the outlet was capped by a septum stopper to prevent the rapid loss of blue) and then syringed into a septum-capped 18- × 150-mm culture tube containing a 0.5-in. stir bar. To this blue solution was added dropwise 5.07 mM of $(NH_4)_2Ce(NO_3)_6$ via a syringe while stirring vigorously. The end point was determined by the color change from blue to amber; the color was best determined using a flashlight because of the slight turbidity of the solution. A total of 0.4 mL of the Ce^{4+} solution was consumed to reach the end point, which corresponds to 1.6 equiv of Ce^{4+} per 1 equiv of initial $(Bu_4N)_5Na_3[(1,5\text{-COD})Ir\cdot P_2W_{15}Nb_3O_{62}]$. The titration was repeated with 3.0 mL of the heteropolyblue; this time 1.3 mL of Ce^{4+} solution was consumed to reach the end point, which corresponds to 1.8 equiv of Ce^{4+} per 1 equiv of initial $(Bu_4N)_5Na_3[(1,5\text{-COD})Ir\cdot P_2W_{15}Nb_3O_{62}]$; the average of the two runs is 1.7 ± 0.1 equiv. However, this number (1.7 equiv) is expected to be underdetermined, since the heteropolyblue is unstable even in the drybox, and thus the true number is almost surely 2.0 equiv of Ce^{4+}, especially since 2.0 equiv of Ce^{4+} corresponds exactly to the number of electrons provided by the 1.0 H_2 consumed (as determined in the independent H_2 uptake experiments). (The instability of the heteropolyblue was independently demonstrated by the following control experiment: 3 mL of heteropolyblue solution was vigorously stirred in a septum-capped 18- × 150-mm tube; 5 min later, the characteristic color of the heteropolyblue lightened significantly.)

Similarly, the heteropolyblue generated under 40 psig of H_2 was titrated with Ce^{4+} in exactly the same manner. The result is the same as that reported above for the heteropolyblue generated under 400 mmHg of H_2, that is, 1.8 ± 0.1 equiv of Ce^{4+}.

Experiments Demonstrating That the $Ir_{\sim 900}$ Nanoclusters (Sample I) Are Negatively Charged. (1) Electrophoresis. To determine the overall charge (positive or negative) on the ca. 30-Å $Ir_{\sim 900}$ nanoclusters (sample I), electrophoresis (the moving boundary method)[37,38] was performed in the drybox by using a U-tube (17 cm high, inner diameter of 8 mm) connected to a side tube (40 cm high) on its base through a stopcock. (A picture of a similar apparatus can be found in ref 37, p 127.) An amber solution of the $Ir_{\sim 900}$ nanoclusters (sample I) in acetonitrile (ca. 2 mg/

(55) Skoog, D. A.; West, D. M. *Analytical Chemistry*; Saunders College Publishing: Philadelphia, PA, 1986; p 310.

mL) was added to the side tube, and the colorless 2 mM Bu_4NPF_6/CH_3CN electrolyte was added to the U-tube, with the stopcock closed. Pt electrodes (ca. 1 mm^2) were then immersed in the electrolyte. After 10 min, the stopcock was carefully opened, and the amber solution was very slowly introduced into the U-tube to give clear boundaries on both sides of the U-tube. Electrophoresis was started when a 24-V dc electric field was applied to the cell through the two electrodes. The experiment was carried out for 2 h at room temperature, again all inside the drybox. The migration rate of the $Ir_{\sim 900}$ nanoclusters was determined on the basis of the average displacement of the boundaries on each side of the U-tube.

In a separate control experiment, designed to demonstrate that the migration of the $Ir_{\sim 900}$ nanoclusters toward the positive electrode was not due to the presence of Bu_4NPF_6 electrolyte, a pure CH_3CN solvent was used to replace the 2 mM Bu_4NPF_6/CH_3CN electrolyte. While the boundary on the side where the negative electrode was placed moved clearly downward (i.e. toward the positive electrode) at the same rate as in the case where 2 mM Bu_4NPF_6/CH_3CN was used, the boundary on the other side (i.e. where the positive electrode was placed) was not clear, presumably due to the ohmic resistance of the pure solvent. This is undoubtedly why it is recommended[38] that such electrophoresis experiments be conducted in an electrolyte having a conductance similar to that of the solution under study.

(2) Reaction of the 30-Å $Ir_{\sim 900}$ Nanoclusters (Sample I) with Ion-Exchange Columns To Confirm That the $Ir_{\sim 900}$ Nanocluster/Polyoxoanion Sample Is Negatively Charged. In the drybox, a cation-exchange column (12 × 100 mm, equipped with a glass frit and stopcock on the bottom) was packed with Amberlite, macroreticular polymer, IRA-400 resin that had been previously washed with aqueous Bu_4NOH until the pH of the wash solution remained strongly basic. Once packed, the now $P–SO_3^-Bu_4N^+$ (P = macroreticular polymer) column was washed with reagent grade acetonitrile until the wash solution was neutral and colorless. Then 2 mL of an amber solution of the 30-Å $Ir_{\sim 900}$ nanoclusters (sample I) was loaded and allowed to pass down through the column. The amber effluent was collected, which was shown by TEM to contain the identical ca. 30-Å $Ir_{\sim 900}$ nanoclusters.

An anion-exchange column (12 × 100 mm, equipped with a glass frit and stopcock on the bottom) of similar proportions was packed with Amberlyst A-27 macroreticular polymer resin in the Cl^- form ($P–NR_3^+Cl^-$; P = macroreticular polymer) and washed with reagent grade acetonitrile until the wash solution was clear. Then 2 mL of an amber solution of the 30-Å $Ir_{\sim 900}$ nanoclusters (sample I) was loaded and allowed to pass down through the $P–NR_3^+Cl^-$ column by opening the stopcock. A colorless effluent was collected, in which no Ir nanoclusters or bulk metal particles were detected by TEM. (The TEM image was indistinguishable from the carbon-film background.) This experiment suggests that the negatively charged, polyoxoanion-adsorbed Ir nanoclusters are bound to $P–NR_3^+$ of the resin. An alternative explanation is that polyoxoanions are replaced by Cl^- and, during the interaction with the ion-exchange resin, that the Ir nanoclusters are decomposed to give tiny metal particles which are then retained on the resin of the column. The later explanation is unlikely, however, as demonstrated by Nakao and co-workers, who examined the resin in a similar experiment (and also in the Cl^- form) using TEM.[41]

Control experiments were also done using much shorter columns (6 × 50 mm) but packed with the same anion- or cation-exchange resin. In one experiment, 1 mL of an amber solution of the 30-Å $Ir_{\sim 900}$ nanoclusters was loaded and passed through an *anion*-exchange $P–NR_3^+Cl^-$ column; a *light-amber* effluent was collected. After passing the effluent from the first column through another new, but otherwise identical, *anion*-exchange column, the light-amber solution turned into a colorless effluent. The colorless effluent was collected and examined by TEM; no Ir nanoclusters or bulk Ir metal particles were found. In a second experiment, 1 mL of an amber solution of the 30-Å $Ir_{\sim 900}$ nanoclusters was loaded and passed, consecutively, through two *cation*-exchange $P–SO_3^-Bu_4N^+$ columns. TEM showed that the amber effluent was unchanged and still contained the same ca. 30-Å $Ir_{\sim 900}$ nanoclusters, confirming the result obtained using the longer (12 × 100 mm) cation-exchange column.

One final control experiment was done using a anion exchange resin *in the BF_4^- form* ($P–NR_3^+BF_4^-$) to see if the same result is obtained as that with the Cl^- form. In a beaker, 2 g of Amberlyst A-27 macroreticular polymer resin in the Cl^- form was stirred with 5 mL of a 0.1 M $AgBF_4$ solution in CH_3CN; thus, Cl^- was replaced by BF_4^- and AgCl precipitate was then removed by washing with acetone until the solution was clear. The above procedure was repeated five times, until all Cl^- was replaced by BF_4^- and any excess $AgBF_4$ was removed. (The absence of Cl^- and Ag^+ was tested by subsequently stirring the resin with a 0.1 M acetone solution of Bu_4NBF_4 in a beaker, then removing an aliquot of the solution from the beaker to a test tube, to which 0.1 M $AgBF_4$ or Bu_4NCl was added, respectively, to ensure that no AgCl precipitate was formed.) The so-obtained BF_4^- form of the resin was then packed in two columns (6 × 50 mm) and further washed with acetone to remove any remaining $AgBF_4$. Finally, the amber solutions of $Ir_{\sim 900}$ nanoclusters were allowed to pass down to the two identical columns consecutively; a colorless effluent was obtained. No Ir nanoclusters or bulk metal particles were found in the effluent by TEM, the same result as seen using the resin in the Cl^- form.

Experiments Demonstrating That the ca. 30-Å $Ir_{\sim 900}$ Nanoclusters (Sample I) Require Excess Polyoxoanion for Their Stability and Nonaggregation. To 2 mL of an amber solution of the ca. 30-Å $Ir_{\sim 900}$ nanoclusters (ca. 1 mg of Ir nanoclusters/mL) was added diethyl ether dropwise until the solution turned cloudy. The solution was then spun at 14 000 rpm to give a dark-brown precipitate and a faint-amber supernatant. The precipitate was redispersed in CH_3CN and sprayed on a carbon film for TEM studies. TEM showed that the previously well-dispersed $Ir_{\sim 900}$ nanoclusters had formed large floccules of $Ir_{\sim 900}$ nanoclusters; moreover, significantly fewer polyoxoanions were present nearby the large floccules (Figure 8b). In contrast, the faint-amber *supernatant* was found to contain well-dispersed discrete ca. 30-Å $Ir_{\sim 900}$ nanoclusters surrounded by polyoxoanions (Figure 8a).

In Situ Generation of 20 ± 3 Å $Ir_{\sim 300}$ Nanoclusters (Sample II) from $(Bu_4N)_5Na_3[(1,5\text{-COD})Ir\cdot P_2W_{15}Nb_3O_{62}]$ (1) and 23 ± 3 Å $Ir_{\sim 400}$ Nanoclusters (Sample III) from $(Bu_4N)_4Na_2[(1,5\text{-COD})Ir\cdot SiW_9Nb_3O_{40}]$ during the Catalytic Hydrogenation of Cyclohexene in Acetone. (For further experimental details relevant to the hydrogenation experiments which follow, see the Experimental Section titled "Standard Conditions for Cyclohexene Hydrogenation Starting with the Precatalyst 1" provided in another paper.[24]) In the drybox, 20.0 ± 2.0 mg ((3.53 ± 0.35) × 10^{-3} mmol) of $(Bu_4N)_5Na_3[(COD)Ir\cdot P_2W_{15}Nb_3O_{62}]$ was dissolved in 2.5 mL of Burdick and Jackson acetone (0.22% H_2O content), followed by the addition of 0.5 mL (4.94 mmol) of purified cyclohexene to give a clear, bright-yellow solution. (The choice of the acetone, its purity, and water content are *crucial variables* in the resultant catalytic activity and, therefore, the resultant nanoclusters. Additional details and data on these variables are presented elsewhere.[24]) The bright-yellow solution (containing 1.2 ± 0.1 mM of $(Bu_4N)_5Na_3[(1,5\text{-COD})Ir\cdot P_2W_{15}Nb_3O_{62}]$ and 1.65 M of cyclohexene) was then transferred to an 18- × 150-mm disposable borosilicate culture tube which contained a 0.5-in. stir bar. The tube was placed in a Fischer–Porter bottle, which had been modified with Swagelok TFE-sealed quick-connects, and was then sealed. The Fischer–Porter bottle was removed from the drybox and then attached to a custom-built, computer-interfaced hydrogenation line (described elsewhere).[24] The Fischer–Porter bottle was purged 15 times with 40 psig of H_2 and shaken vigorously for 30 s to allow for the equilibration between hydrogen gas and the liquid reaction mixture. Then, the reaction was started by stirring the solution vigorously. The H_2 pressure vs time data were collected and analyzed as detailed elsewhere.[24] The above *hydrogenation* procedure has been repeated more than 100 times and by two different researchers;[23b,c,24] the hydrogenation results are reproducible within 10% *provided* one uses the *same batch* of acetone (i.e., with the same purity and same water content) and if the concentrations and other variables are kept constant.

As the reaction proceeded, the originally clear-yellow solution gradually turned turbid-amber and then an intense blue color (due to the formation of heteropolyblue[27]) when the cyclohexene hydrogenation reaction was ca. 90% complete. After the reaction was stopped, the reaction product solution was brought into the drybox and filtered through Whatman No. 2 paper to give a clear filtrate and a brown precipitate; no bulk Ir(0) metal particles were observed. The color of the filtrate depended on the extent of the hydrogenation reaction (light-yellow-green if the reaction is <80% complete and blue if the reaction is >90% complete), but the blue color gradually turned amber in the drybox within ca. 30 min once the H_2 pressure was released. The brown precipitate was soluble in acetone or acetonitrile to give an amber solution which appears "homogeneous" to the naked eye. The clear amber acetone solution was sprayed on a carbon film and then characterized by TEM (Figure 10), which showed the presence of numerous ca. 20-Å Ir nanoclusters. However, TEM (Figure H, supplementary material) of the light-yellow filtrate (collected when the reaction was stopped at 50% completion) showed significantly fewer Ir nanoclusters. Both the amber solution and the clear-yellow filtrate were also characterized by visible spectroscopy (Figure I, supplementary material).

As an augment to TEM, ultracentrifugation was used as an alternative way to detect the Ir nanoclusters in solution. In the drybox, the clear-amber solution (ca. 1 mg of brown precipitate/mL of acetone and, in a separate experiment, ca. 1 mg of brown precipitate/mL of CH_3CN) was placed in a small double-sector quartz cell which was specially designed for ultracentrifuge molecular-weight measurements. The cell was removed from the drybox, loaded in a rotor in the ultracentrifuge, and then spun at 20 000 rpm under vacuum. After 10 min, absorbance in the visible range was diminished. It was found, after the experiment was finished and the cell was carefully removed, that the previously amber solution had turned into a clear, colorless supernatant (the polyoxoanions) and a dark-brown precipitate at the bottom of the cell (the Ir nanoclusters). (If the cell was shaken, the amber solution reforms.) In a separate experiment, a solution molecular-weight measurement was conducted with the addition of $Bu_4N^+PF_6^-$ as an electrolyte and in CH_3CN; $\overline{M}_r$ of the 20-Å Ir nanoclusters is $(8.6 \pm 4.0) \times 10^4$ (Figure J, supplementary material). The MW of the polyoxoanions included in the Ir nanocluster sample is 10 800 ± 2000 (Figure K, supplementary material). (Details of the molecular-weight measurements were given earlier in the Experimental, under Solution Molecular-Weight Measurements.)

In Situ Generation of 23 ± 3 Å $Ir_{\sim 400}$ Nanoclusters from $(Bu_4N)_4Na_2[(1,5\text{-COD})Ir{\cdot}SiW_9Nb_3O_{40}]$ during the Catalytic Hydrogenation of Cyclohexene in Acetone. The catalytic cyclohexene hydrogenation and the in situ generation of Ir nanoclusters starting from 1.0 mM $(Bu_4N)_4Na_2[(1,5\text{-COD})Ir{\cdot}SiW_9Nb_3O_{40}]$ was carried out in a a manner exactly analogous to that described above for $(Bu_4N)_5Na_3[(COD)Ir{\cdot}P_2W_{15}Nb_3O_{62}]$. As in the case of $(Bu_4N)_5Na_3[(COD)Ir{\cdot}P_2W_{15}Nb_3O_{62}]$, the hydrogenation reaction solution gradually turned a turbid-amber color as the cyclohexene hydrogenation proceeded. But no blue color was ever observed and no bulk Ir metal particles were ever observed. TEM (Figure 11) indicated the presence of ca. 22.6 ± 3.3 Å Ir nanoclusters in the cloudy, amber product solution.

Control Experiment Consisting of the in Situ Generation of Polyoxoanion-Free 14 ± 4 Å $Ir_{\sim 100}$ Nanoclusters (Sample IV) from $[(1,5\text{-COD})Ir{\cdot}(acetone)_2]BF_4$ plus 0, 1, or 2 Equiv of Bu_4NOH during the Catalytic Hydrogenation of Cyclohexene in Acetone. In the drybox, 10.0 mg (0.0149 mmol) of $[(1,5\text{-COD})IrCl]_2$ was suspended in 10 mL of Burdick and Jackson acetone in a beaker. Then, 5.8 mg (0.03 mmol, 2.0 equiv) of $AgBF_4$ was added to give a white precipitate (AgCl) and, after stirring for 10 min, the reaction mixture was filtered through filter paper (Whatman No. 2) to give a clear-yellow solution. The filter paper was washed with acetone and the washings were combined with the yellow filtrate, which was then placed under a vacuum at ambient temperature and evacuated to dryness, all while still inside the drybox. The dry residue was redissolved in Burdick and Jackson acetone in a volumetric flask to give 5.00 mL (5.6 mM) of $[(1,5\text{-COD})Ir{\cdot}(acetone)_2]BF_4$. (Note that the $(1,5\text{-COD})Ir(acetone)_2^+$ complex cannot be crystallized,[56] in contrast to the related $(1,5\text{-COD})Ir(CH_3CN)_2^+$ complex.[57]) To 1.0 mL of the freshly prepared acetone solution of $[(1,5\text{-COD})Ir{\cdot}(acetone)_2]BF_4$ in a borosilicate culture tube was added 1.5 mL of acetone followed by the addition (in separate experiments) of 0 μL, 3.9 μL (5.95×10^{-3} mmol, 1.2 equiv), or 6.5 μL (9.92×10^{-3} mmol, 2.0 equiv) of Bu_4NOH (40% in H_2O, 1.53 M). Then cyclohexene (0.5 mL) was added to the culture tube, which was placed in a Fischer–Porter bottle. The Fischer–Porter bottle was sealed, removed from the drybox, and attached to the hydrogenation line via the quick-connects, and the reaction (starting with 1.8 mM $[(1,5\text{-COD})Ir{\cdot}(acetone)_2]BF_4$, 1.6 M cyclohexene, and 40 psig of H_2 in the presence of 0, 1, or 2 equiv of Bu_4NOH) was initiated and carried out in the same manner as that described for $(Bu_4N)_5Na_3[(1,5\text{-COD})Ir{\cdot}P_2W_{15}Nb_3O_{62}]$. In the absence of Bu_4NOH, the reaction proceeded essentially immediately and without an induction period, but with the formation of bulk Ir(0) particles and to a colorless solution. In the experiment with 1 equiv of Bu_4NOH, the reaction started with an induction period, but bulk Ir(0) metal particles are still observed at the end of reaction. However, in the presence of 2 equiv of $(Bu_4N)OH$, the reaction proceeded with a much longer induction period and slower rate, and the original clear-yellow solution gradually turned to yellow-brown (no precipitate was observed). When repeated, the reaction with 2.0 equiv of Bu_4NOH was irreproducible, exhibiting unpredictable induction periods (from 0 to 2 h) and reaction rates (from 10 to 40 h for the completion of cyclohexene hydrogenation). Thus, the hydrogenation progress curve shown in Figure L is for illustrative purposes only. The product solution from the reaction with addition of 2 equiv of Bu_4NOH was characterized by TEM (Figure 12).

Control Experiments Demonstrating That Only Polyoxoanions with Surface-Oxygen Basicity (i.e., $P_2W_{15}Nb_3O_{62}^{9-}$ and $SiW_9Nb_3O_{40}^{7-}$) Provide $Ir_{\sim 300}$ Nanoclusters and Avoid the Precipitation of Bulk Ir(0) Metal. In the drybox, 69 mg (0.012 mmol, 2 equiv) of $(Bu_4N)_6P_2W_{18}O_{62}$ was added to 3.0 mL of an orange-yellow acetone solution of $[(1,5\text{-COD})Ir(acetone)_2]BF_4$ (1.8 mM) and 1.65 M cyclohexene in a 18- × 150-mm borosilicate culture tube containing a 0.5-in. stir bar. The culture tube was then placed in the Fischer–Porter bottle, which was then brought out of the drybox, and connected to the H_2 line, and the hydrogenation reaction was carried out under the standard procedure and conditions as described above. Immediate H_2 uptake was observed without an induction period; black bulk Ir(0) metal particles were found, and the reaction solution had turned to an intense blue indicative of a reduced, W^V-containing "heteropolyblue",[27] $(Bu_4N)_6H_x[P_2W^{VI}_{18-x}W^V_xO_{62}]$.

Understanding the Induction Period and Autocatalysis. Experiments Testing for Iridium(0) $Ir_{\sim 300}$ Nanocluster Formation from the Dissociation of Precatalyst 1 to $(1,5\text{-COD})Ir(solvent)_2^+$ and $P_2W_{15}Nb_3O_{62}^{9-}$) and Then the Reduction of $(1,5\text{-COD})Ir(solvent)_2^+$ to Ir(0). The solvent-dependence studies provided below (i.e., the shorter induction period and bulk Ir(0) formation in more coordinating solvents such as CH_3CN) initially suggested the dissociation of $(1,5\text{-COD})Ir{\cdot}P_2W_{15}Nb_3O_{62}^{8-}$ (**1**), to $(1,5\text{-COD})Ir(solvent)_2^+$ and $P_2W_{15}Nb_3O_{62}^{9-}$ (with $K_{dissoc} \ll 1$ according to all the solution spectroscopic data for **1**).[25] If true, then added $P_2W_{15}Nb_3O_{62}^{9-}$ should greatly increase the length of the induction period if not essentially stop the reaction (as a simple equilibrium calculation illustrates, so long as $K_{dissoc} \ll 1$). Oppositely, added $(1,5\text{-COD})Ir(solvent)_2^+$ should significantly reduce the induction period. The additional prediction is that the H_2 uptake rate after the induction period should be essentially unchanged. These predictions are tested via the experiments which follow.

(a) Inhibition of Cyclohexene Hydrogenation by Added $(Bu_4N)_9P_2W_{15}Nb_3O_{62}$. In the drybox, 23.0 mg (4.1×10^{-3} mmol) of $(Bu_4N)_5Na_3[(1,5\text{-COD})Ir{\cdot}P_2W_{15}Nb_3O_{62}]$ was dissolved in 2.5 mL of Burdick and Jackson acetone in a standard borosilicate culture tube followed by the addition of 0.17 g (0.03 mmol, 7.3 equiv) of $(Bu_4N)_9P_2W_{15}Nb_3O_{62}$ and 0.5 mL of cyclohexene to give a clear-yellow solution. The culture tube was placed inside a Fischer–Porter bottle, and the bottle was removed from the drybox and attached to the hydrogenation apparatus. The cyclohexene hydrogenation reaction was then initiated with 40 psig of H_2 and vigorous shaking and stirring according to the standard conditions and procedures. No H_2 loss is observed even after 22 h, 11 times the normal 2.0-h induction period. A check by ^1H NMR confirmed the absence of product (cyclohexane) in the reaction mixture.

(b) Acceleration of Autocatalysis by Added $[(1,5\text{-COD})Ir(acetone)_2]SbF_6$. (i) In Situ Preparation of $[(1,5\text{-COD})Ir(acetone)_2]SbF_6$. In the drybox, 0.101 g of $[(1,5\text{-COD})IrCl_2]$ (0.15 mmol) was dissolved in ca. 1 mL of CH_2Cl_2 followed by the addition of 10 mL of Burdick and Jackson acetone to give an orange-red solution. To this solution was added 0.103 g of $AgSbF_6$ (0.30 mmol, 2.0 equiv) to give a white precipitate and a yellow solution. After the reaction mixture was stirred for an additional 20 min to ensure complete reaction, the solution was filtered through Whatman No. 5 paper and the filter paper was then washed with three 5-mL portions of Burdick and Jackson acetone. The washings were combined with the yellow filtrate, which was then placed under a vacuum at ambient temperature and evacuated to dryness, all while still inside the drybox. The dry residue was redissolved in Burdick and Jackson acetone in a volumetric flask to give 5.00 mL of a 2.0 mM yellow solution of in situ generated $[(1,5\text{-COD})Ir(acetone)_2]SbF_6$. (Note that, again, the $(1,5\text{-COD})Ir(acetone)_2^+$ complex cannot be crystallized,[56] in contrast to the related $(1,5\text{-COD})Ir(CH_3CN)_2^+$ complex.[57])

(ii) Cyclohexene Hydrogenation Experiment with Added $[(1,5\text{-COD})Ir(acetone)_2]SbF_6$. In the drybox, 20.6 mg (3.6×10^{-3} mmol, 1.2 mM) of $(Bu_4N)_5Na_3[(1,5\text{-COD})Ir{\cdot}P_2W_{15}Nb_3O_{62}]$ was dissolved in 2.5 mL of Burdick and Jackson acetone in the standard borosilicate culture tube followed by the addition of 0.04 equiv (75 μL, 2 mM) of $[(1,5\text{-COD})Ir(acetone)_2]SbF_6$ and 0.5 mL (4.94 mmol, 1.65 M) of fresh cyclohexene to give a orange-red solution. The culture tube was placed inside a Fischer–Porter bottle, and the bottle was removed form the drybox and attached to the hydrogenation apparatus. The cyclohexene hydrogenation reaction was then initiated with 40 psig of H_2 and vigorous shaking and stirring according to the standard conditions and procedures. A ca. 40% shorter (1.25 h) induction period was observed, followed by an essentially normal H_2 uptake rate of 1.1 mmol H_2/h within experimental error. As the

(56) Sievert, A. C.; Muetterties, E. L. *Inorg. Chem.* **1981**, *20*, 489.
(57) Day, V. W.; Klemperer, W. G.; Main, D. J. *Inorg. Chem.* **1990**, *29*, 2345.

reaction proceeded, the reaction solution turned cloudy and an intense blue color was observed, identical to a standard conditions cyclohexene hydrogenation.

A control experiment employing a 1.0 mM orange-yellow solution of $[(1,5\text{-COD})Ir(acetone)_2]SbF_6$ and 1.65 M cyclohexene in Burdick and Jackson acetone showed that, in an otherwise standard conditions cyclohexene hydrogenation, the hydrogenation reaction proceeded rapidly, *without an induction period*, that bulk Ir(0) metal particles were observed, and that the final solution had turned colorless.

Quantitative GEAR/GIT Curve Fitting of the H_2 Pressure Loss Curve Demonstrating That Only Autocatalysis Accounts for the Observed Induction Period. Hydrogen pressure loss data was analyzed using the numerical integration package[58] containing Gear[58b] and GIT[58c] by a four-step minimum kinetic model.[23b,c] The key result, previously presented elsewhere,[23c] is that a good fit can only be obtained if an autocatalytic step is included in the kinetic model. See the text for additional discussion.

Acknowledgment. We are indebted to Dr. Eric Schabtach (University of Oregon Electron Microscope Facility) who obtained the transmission electron micrographs and electron diffraction patterns shown herein. Dr. D. K. Lyon is acknowledged for doing H_2 uptake stoichiometry experiments and other control experiments cited along with his name. We thank Dr. F. Dong for his assistance in ultracentrifugation MW measurements and Professor Bönnemann for sending us a detailed description regarding the preparation of their Ir nanoclusters. Financial support was provided by the Department of Energy, Chemical Sciences Division, Office of Basic Energy (Grant DOE FG06-089ER13998).

(58) (a) McKinney, R. J.; Weigert, F. J. Quantum Chemistry Program Exchange, Program No. QCMP022. (b) Stabler, R. N.; Chesick, J. *Int. J. Kinet.* **1978**, *10*, 461. (c) Weigert, F. *J. Comput. Chem.* **1987**, *11*, 272.

Supplementary Material Available: Figures A and B showing transmission electron micrographs of the $Ir_{\sim 900}$ nanoclusters (from acetone solution prior to isolation), Figure C showing the UV-visible spectrum of the $Ir_{\sim 900}$ nanoclusters in acetone solution together with those of $(Bu_4N)_5Na_3[(COD)Ir{\cdot}P_2W_{15}Nb_3O_{62}]$ and $(Bu_4N)_{12}H_4P_4W_{30}Nb_6O_{123}$ for comparison, Figure D showing a plot of $\ln(A)$ vs r^2 from the ultracentrifugation molecular-weight measurement for the $Ir_{\sim 900}$ nanoclusters, Figure E showing the IR spectrum (KBr) of the $Ir_{\sim 900}$ nanoclusters, Figure F showing the FAB-MS of the $Ir_{\sim 900}$ nanoclusters, Figure G showing a plot of $\ln(A)$ vs r^2 from the ultracentrifugation molecular-weight measurement for the polyoxoanions that are part of the $Ir_{\sim 900}$ nanoclusters, Figure H showing the transmission electron micrograph of the filtrate from the cyclohexene hydrogenation product solution starting with 1.0 mM $(Bu_4N)_5Na_3[(1,5\text{-}COD)Ir{\cdot}P_2W_{15}Nb_3O_{62}]$ and 1.65 M cyclohexene in acetone under 40 psig of H_2, Figure I showing visible spectra of the $Ir_{\sim 300}$ nanoclusters in acetone, Figure J showing a plot of $\ln(A)$ vs r^2 from the ultracentrifugation molecular-weight measurement for the $Ir_{\sim 300}$ nanoclusters, Figure K showing a plot of $\ln(A)$ vs r^2 from the ultracentrifugation molecular-weight measurement for the polyoxoanions that are part of the $Ir_{\sim 300}$ nanoclusters, Figure L showing the effect of Bu_4NOH addition to $[(1,5\text{-COD})Ir{\cdot}(acetone)_2]BF_4$ on the cyclohexene hydrogenation in acetone, and Figure M showing the effect of $[Ir(1,5\text{-COD})(acetone)_2]SbF_6$ addition on the cyclohexene hydrogenation reaction starting with 1 mM $(Bu_4N)_5Na_3[(1,5\text{-COD})Ir{\cdot}P_2W_{15}Nb_3O_{62}]$ (13 pages). This material is contained in many libraries on microfiche, immediately follows this article in the microfilm version of the journal, and can be ordered from the ACS; see any current masthead page for ordering information.